Muon capture on light isotopes measured with the Double Chooz detector

Citation: Abe, Y., T. Abrahao, H. Almazan, C. Alt, S. Appel, J. C. Barriere, E. Baussan, et al. "Muon Capture on Light Isotopes Measured with the Double Chooz Detector." Physical Review C 93, no. 5 (May 12, 2016). © 2016 American Physical Society

As Published: http://dx.doi.org/10.1103/PhysRevC.93.054608

Publisher: American Physical Society

Persistent URL: http://hdl.handle.net/1721.1/102655

Version: Final published version: final published article, as it appeared in a journal, conference proceedings, or other formally published context

Muon capture on light isotopes measured with the Double Chooz detector

Y. Abe,[27] T. Abrahão,[5] H. Almazan,[20] C. Alt,[1] S. Appel,[29] J. C. Barriere,[14] E. Baussan,[22] I. Bekman,[1] M. Bergevin,[9] T. J. C. Bezerra,[25] L. Bezrukov,[13] E. Blucher,[6] T. Brugière,[22] C. Buck,[20] J. Busenitz,[2] A. Cabrera,[4] L. Camilleri,[8] R. Carr,[8] M. Cerrada,[7] E. Chauveau,[25] P. Chimenti,[31] A. P. Collin,[20] E. Conover,[6] J. M. Conrad,[19] J. I. Crespo-Anadón,[7] K. Crum,[6] A. S. Cucoanes,[23,*] E. Damon,[10] J. V. Dawson,[4] H. de Kerret,[4] J. Dhooghe,[9] D. Dietrich,[30] Z. Djurcic,[3] J. C. dos Anjos,[5] M. Dracos,[22] A. Etenko,[18] M. Fallot,[23] J. Felde,[9,†] S. M. Fernandes,[2] V. Fischer,[14] D. Franco,[4] M. Franke,[29] H. Furuta,[25] I. Gil-Botella,[7] L. Giot,[23] M. Göger-Neff,[29] H. Gomez,[4] L. F. G. Gonzalez,[32] L. Goodenough,[3] M. C. Goodman,[3] N. Haag,[29] T. Hara,[17] J. Haser,[20] D. Hellwig,[1] M. Hofmann,[29] G. A. Horton-Smith,[15] A. Hourlier,[4] M. Ishitsuka,[27] J. Jochum,[30] C. Jollet,[22] F. Kaether,[20] L. N. Kalousis,[33] Y. Kamyshkov,[24] M. Kaneda,[27] D. M. Kaplan,[12] T. Kawasaki,[16] E. Kemp,[32] D. Kryn,[4] M. Kuze,[27] T. Lachenmaier,[30] C. E. Lane,[10] T. Lasserre,[4,14] A. Letourneau,[14] D. Lhuillier,[14] H. P. Lima Jr,[5] M. Lindner,[20] J. M. López-Castaño,[7] J. M. LoSecco,[21] B. Lubsandorzhiev,[13] S. Lucht,[1] J. Maeda,[28,‡] C. Mariani,[33] J. Maricic,[10,§] J. Martino,[23] T. Matsubara,[28] G. Mention,[14] A. Meregaglia,[22] T. Miletic,[10] R. Milincic,[10,§] A. Minotti,[22] Y. Nagasaka,[11] D. Navas-Nicolás,[7] P. Novella,[7,‖] L. Oberauer,[29] M. Obolensky,[4] A. Onillon,[4] A. Osborn,[24] C. Palomares,[7] I. M. Pepe,[5] S. Perasso,[4] A. Porta,[23] G. Pronost,[23] J. Reichenbacher,[2] B. Reinhold,[20,§] M. Röhling,[30] R. Roncin,[4] B. Rybolt,[24] Y. Sakamoto,[26] R. Santorelli,[7] A. C. Schilithz,[5] S. Schönert,[29] S. Schoppmann,[1] M. H. Shaevitz,[8] R. Sharankova,[27] D. Shrestha,[15] V. Sibille,[14] V. Sinev,[13] M. Skorokhvatov,[18] E. Smith,[10] M. Soiron,[1] J. Spitz,[19] A. Stahl,[1] I. Stancu,[2] L. F. F. Stokes,[30] M. Strait,[6,¶] F. Suekane,[25] S. Sukhotin,[18] T. Sumiyoshi,[28] Y. Sun,[2,§] R. Svoboda,[9] K. Terao,[19] A. Tonazzo,[4] H. H. Trinh Thi,[29] G. Valdiviesso,[5] N. Vassilopoulos,[22] C. Veyssiere,[14] M. Vivier,[14] F. von Feilitzsch,[29] S. Wagner,[5] N. Walsh,[9] H. Watanabe,[20] C. Wiebusch,[1] M. Wurm,[30,#] G. Yang,[3,12] F. Yermia,[23] and V. Zimmer[29]

(Double Chooz Collaboration)

[1] *III. Physikalisches Institut, RWTH Aachen University, 52056 Aachen, Germany*

[2] *Department of Physics and Astronomy, University of Alabama, Tuscaloosa, Alabama 35487, USA*

[3] *Argonne National Laboratory, Argonne, Illinois 60439, USA*

[4] *AstroParticule et Cosmologie, Université Paris Diderot, CNRS/IN2P3, CEA/IRFU, Observatoire de Paris, Sorbonne Paris Cité, 75205 Paris Cedex 13, France*

[5] *Centro Brasileiro de Pesquisas Físicas, Rio de Janeiro, RJ 22290-180, Brazil*

[6] *The Enrico Fermi Institute, The University of Chicago, Chicago, Illinois 60637, USA*

[7] *Centro de Investigaciones Energéticas, Medioambientales y Tecnológicas, CIEMAT, 28040 Madrid, Spain*

[8] *Columbia University, New York, New York 10027, USA*

[9] *University of California, Davis, California 95616, USA*

[10] *Department of Physics, Drexel University, Philadelphia, Pennsylvania 19104, USA*

[11] *Hiroshima Institute of Technology, Hiroshima 731-5193, Japan*

[12] *Department of Physics, Illinois Institute of Technology, Chicago, Illinois 60616, USA*

[13] *Institute of Nuclear Research of the Russian Academy of Sciences, Moscow 117312, Russia*

[14] *Commissariat à l'Energie Atomique et aux Energies Alternatives, Centre de Saclay, IRFU, 91191 Gif-sur-Yvette, France*

[15] *Department of Physics, Kansas State University, Manhattan, Kansas 66506, USA*

[16] *Department of Physics, Kitasato University, Sagamihara 252-0373, Japan*

[17] *Department of Physics, Kobe University, Kobe 657-8501, Japan*

[18] *NRC Kurchatov Institute, 123182 Moscow, Russia*

[19] *Massachusetts Institute of Technology, Cambridge, Massachusetts 02139, USA*

[20] *Max-Planck-Institut für Kernphysik, 69117 Heidelberg, Germany*

[21] *University of Notre Dame, Notre Dame, Indiana 46556, USA*

[22] *IPHC, Université de Strasbourg, CNRS/IN2P3, 67037 Strasbourg, France*

[23] *SUBATECH, CNRS/IN2P3, Université de Nantes, Ecole des Mines de Nantes, 44307 Nantes, France*

[24] *Department of Physics and Astronomy, University of Tennessee, Knoxville, Tennessee 37996, USA*

[25] *Research Center for Neutrino Science, Tohoku University, Sendai 980-8578, Japan*

[26] *Tohoku Gakuin University, Sendai 981-3193, Japan*

[27] *Department of Physics, Tokyo Institute of Technology, Tokyo 152-8551, Japan*

[28] *Department of Physics, Tokyo Metropolitan University, Tokyo, 192-0397, Japan*

[29] *Physik Department, Technische Universität München, 85748 Garching, Germany*

[30] *Kepler Center for Astro and Particle Physics, Universität Tübingen, 72076 Tübingen, Germany*

[31] *Universidade Federal do ABC, UFABC, Santo André, São Paulo 09210-580, Brazil*

[32] *Universidade Estadual de Campinas-UNICAMP, Campinas, São Paulo 13083-970, Brazil*

[33] *Center for Neutrino Physics, Virginia Tech, Blacksburg, Virginia 24061, USA*

(Received 23 December 2015; revised manuscript received 9 March 2016; published 12 May 2016)

Using the Double Chooz detector, designed to measure the neutrino mixing angle θ_{13}, the products of μ^- capture on ^{12}C, ^{13}C, ^{14}N, and ^{16}O have been measured. Over a period of 489.5 days, 2.3×10^6 stopping cosmic μ^- have been collected, of which 1.8×10^5 captured on carbon, nitrogen, or oxygen nuclei in the inner detector scintillator or acrylic vessels. The resulting isotopes were tagged using prompt neutron emission (when applicable), the subsequent β decays, and, in some cases, β-delayed neutrons. The most precise measurement of the rate of $^{12}\mathrm{C}(\mu^-,\nu)^{12}\mathrm{B}$ to date is reported: $6.57^{+0.11}_{-0.21} \times 10^3$ s^{-1}, or $(17.35^{+0.35}_{-0.59})$% of nuclear captures. By tagging excited states emitting γs, the ground state transition rate to ^{12}B has been determined to be $5.68^{+0.14}_{-0.23} \times 10^3$ s^{-1}. The heretofore unobserved reactions $^{12}\mathrm{C}(\mu^-,\nu\alpha)^8\mathrm{Li}$, $^{13}\mathrm{C}(\mu^-,\nu n\alpha)^8\mathrm{Li}$, and $^{13}\mathrm{C}(\mu^-,\nu n)^{12}\mathrm{B}$ are measured. Further, a population of βn decays following stopping muons is identified with 5.5σ significance. Statistics limit our ability to identify these decays definitively. Assuming negligible production of ^{8}He, the reaction $^{13}\mathrm{C}(\mu^-,\nu\alpha)^9\mathrm{Li}$ is found to be present at the 2.7σ level. Limits are set on a variety of other processes.

DOI: 10.1103/PhysRevC.93.054608

I. INTRODUCTION

A μ^- that stops in a material is rapidly captured into an atomic orbital and subsequently rapidly cascades down into the 1s state (referred to herein as *atomic capture*). From this state, a muon can either decay or may undergo *nuclear capture*. This process is the muon analog to the electron capture decay that proton-rich isotopes undergo. However, muon capture is always energetically favorable and therefore competes with muon decay regardless of the isotope. The large mass of the muon also makes available a wide variety of final states. In addition to converting a proton to a neutron, nucleons can be ejected from the nucleus [1].

Measurements of the probabilities of these various states are interesting for reactor neutrino experiments, for example, because they form backgrounds to the inverse β decay reaction. In particular, production of isotopes that undergo β-delayed neutron emission (henceforth called βn isotopes) forms a nearly irreducible background, since the inverse β decay signal is a positron and a neutron. Production of ordinary β-unstable isotopes is less troublesome for reactor neutrino experiments, but as these isotopes often have Q_β values far in excess of natural radioactivity, they will contribute to the high-energy accidental spectrum of delayed-coincidence searches. In addition, it could be relevant for experiments whose signal is a single event, for instance electron recoil.

Muon capture measurements provide input for understanding nuclear structure and can be used to validate models of neutrino cross sections, such as PQRPA. This is particularly true for measurements of production of the exclusive states of ^{12}B [2]. The reaction is a close analog to neutrino capture interactions such as those that will be observed in the event of a galactic supernova. In each, about ∼20 MeV is available for excitations, often leading to nucleon emission and a variety of excited states. Another similar situation occurs in the baryon-number violating process of proton or bound-neutron decay to invisible products, as is being studied by several large underground detectors. While not currently a competitive technique, the rate of $^{12}\mathrm{C}(\mu^-,\nu)^{12}\mathrm{B}_{\mathrm{g.s.}}$ has also been used as input for measurement of g_P [3].

The structure of this paper is as follows. In Sec. II, the detector is described, including its isotopic composition. In Sec. III, the rate of stopping muons in a clean sample of events (the "high-purity sample") is found. This rate is used in Sec. IV to find the probabilities of forming ^{12}B and ^{13}B. These probabilities are then used in Sec. V to find the stopping muon rate in a less clean, but three times larger, sample of stopping muons (the "loose sample"). Total nuclear and atomic capture rates for each relevant isotope, along with their systematic errors, are tabulated here. This larger sample is used to analyze production of isotopes in the following sections.

Analysis of all the rest of the isotopes follows: βn emitters are presented in Sec. VI, the ^{12}Be decay chain in Sec. VII, and a variety of simple β decays in Sec. VIII. Section IX shows exclusive measurements of ^{12}B states. Finally, Sec. X concludes.

II. DETECTOR

The Double Chooz experiment consists of two nearly identical detectors, the *near* and *far* detectors, placed 400 m and 1 km, respectively, from a commercial nuclear reactor. It has been described in detail elsewhere [4]. It consists of four concentric liquid zones, passive shielding, and an outer veto of plastic scintillator. The innermost three zones form one optical volume as follows:

(i) The *neutrino target* is a cylinder with height 2.5 m and diameter 2.3 m filled with gadolinium-loaded liquid

*Present address: ELI-NP, "Horia Hulubei" National Institute of Physics and Nuclear Engineering, 077125 Bucharest-Magurele, Romania.

†Present address: Department of Physics, University of Maryland, College Park, Maryland 20742, USA.

‡Present address: Department of Physics, Kobe University, Kobe, 658-8501, Japan.

§Present address: Department of Physics, and Astronomy, University of Hawaii at Manoa, Honolulu, Hawaii 96822, USA.

‖Present address: Instituto de Física Corpuscular, IFIC (CSIC/UV), 46980 Paterna, Spain.

¶Corresponding author: strait@hep.uchicago.edu.

#Present address: Institut für Physik and Excellence Cluster PRISMA, Johannes Gutenberg-Universität Mainz, 55128 Mainz, Germany.

scintillator. The gadolinium allows for efficient and nearly background-free detection of neutrons because of its large thermal cross section and the 8 MeV of γs released from each capture, which rise well above the background from natural radioactivity.

(ii) The γ *catcher* is a cylindrical layer with thickness 0.6 m filled with liquid scintillator without gadolinium. Its purpose is to provide an interaction region for γs produced in the neutrino target.

(iii) The *buffer* is a 1.1-m layer of nonscintillating mineral oil surrounding the neutrino target and γ catcher. In it are mounted 390 10″ PMTs. The oil shields the scintillator from PMT glass radioactivity as well as externally produced γs and neutrons.

The neutrino target is separated from the γ catcher by a clear acrylic vessel with thickness of 8 mm, and the γ catcher from the buffer by an acrylic vessel of thickness 12 mm. The neutrino target, γ catcher and buffer are collectively called the *inner detector*.

The inner detector is contained in a steel vessel, outside of which is a 0.5-m-thick layer of liquid scintillator called the *inner veto*, in which 78 8″ PMTs are mounted. The inner veto is, in turn, surrounded by 15 cm of passive steel shielding. Above the steel shield, the *outer veto*, consisting of several large-area plastic scintillator panels, provides additional muon tagging and tracking.

The far detector is located under a hill with 300 m water equivalent overburden. The muon rate through the inner veto is 40 Hz, of which about 0.3% stop in the neutrino target or γ catcher. Only data from the far detector are included in this analysis. The far detector has been running since 2011. The first 489.5 days of livetime are used in this analysis.

Muon capture can be observed with, in principle, up to a sevenfold coincidence:

(1) muon track;

(2) muonic x rays and Auger electrons from the atomic cascade: $\ll 1$ ns after stop;

(3) capture nuclear recoil: O(1 μs) after the atomic cascade;

(4) γ/charged particles from nuclear de-excitation: *usually* $\ll 1$ ns after capture, but > 1 μs in some cases;

(5) capture of neutrons from nuclear de-excitation: 10–100 μs after μ capture;

(6) β or βn decay of daughter nucleus: 10 ms–10 s after μ capture;

(7) capture of neutron from βn decay: 10–100 μs after βn decay.

Signals 1, 5, 6, and 7 are easily observable in Double Chooz. In particular, neutrons (5 and 7) can be detected by the 2.22-MeV γ resulting from capture on hydrogen in either the neutrino target or γ catcher, or by the 8-MeV of γs resulting from capture on gadolinium in the neutrino target. The efficiency for observing these neutrons is acceptable, but lower than the neutron efficiency of the Double Chooz neutrino analysis because the trigger is not fully efficient following large signals such as muons.

Signal 4 with γs is observable with some complications due to muon-induced deadtime and baseline shifts. Signal 2 is not observable because it is always prompt and completely masked by the muon track's light. It would be easily observable in a segmented detector, however, at least for high Z targets (for instance, gadolinium gives muonic x rays at 4.7 and 1.8 MeV, and about 1 MeV of softer x rays and Auger electrons). Signals 3 and 4 with charged particles are not visible because the scintillation is highly quenched.

In Double Chooz, therefore, the coincidence can be up to fivefold, but as it turns out, no reactions using all five signals are practical to observe. Examples do exist for $1+6$ (track + β, such as ^{12}B produced by ^{12}C, Sec. IV), $1+5+6$ (...with a neutron, such as ^{12}B produced by ^{13}C, same section), $1+6+7$ (track + βn, such as ^{9}Li produced by ^{13}C, see Sec. VI), $1+5+6+7$ (...with a neutron, such as ^{17}N produced by ^{18}O, same section), or $1+4+6$ (track + γ + β, excited states of ^{12}B, see Sec. IX).

TABLE I. β-decaying isotopes that can be produced by muon capture in Double Chooz. The lower left box contains those that can be produced from ^{12}C.

		^{12}N	•	—	—	^{16}N	^{17}N	^{18}N
^{9}C	•	•	—	—	•	^{15}C	^{16}C	^{17}C
^{8}B		—	—	^{12}B	^{13}B	^{14}B	^{15}B	
•		—	•	^{11}Be	^{12}Be		^{14}Be	
—	—	^{8}Li	^{9}Li		^{11}Li			
	^{6}He		^{8}He					

A. Candidate isotopes

The most common isotope in Double Chooz is ^{12}C, but ^{13}C, ^{14}N, ^{16}O, ^{17}O, and ^{18}O are also present in relevant quantities. While there is also hydrogen in the detector, μ^- never undergoes nuclear captures on it. In the case that the muon captures atomically on hydrogen, it is always quickly picked off by a heavier element [1].

Some previous data exist for partial capture rates in ^{12}C, ^{14}N, and ^{16}O, as summarized in Ref. [1]. Some newer results on nitrogen and oxygen are also available [5,6]. For ^{13}C, no previous measurements of partial capture rates are available.

Tables I and II display all isotopes that could possibly be observed in Double Chooz from muon capture on any stable isotope of carbon, nitrogen, or oxygen. This is the same as listing all possible muon-capture products of ^{18}O, i.e., anything that can be made by removing zero or more nucleons from ^{18}N. In Table I, isotopes analyzed in this paper are shown nonitalicized. Stable isotopes are shown as long dashes (—) and those that decay too slowly as dots (•). Isotopes that undergo strong decays are not shown. Isotopes that can only be formed from ^{17}O or ^{18}O are italicized. Because of the rarity of these two parent isotopes, their daughters are not measured, but some are taken into account when measuring other isotopes.

B. About carbon

The neutrino target and γ catcher scintillators and acrylic vessels contain 24.0 tons of carbon. From EA-IRMS measurements, the molar ^{13}C fractions of the Double Chooz scintillators are known to be 1.0925(1)% for the neutrino target and 1.0906(1)% for the γ catcher. The atomic capture rates for different isotopes of an element are identical. The

TABLE II. Decay characteristics [7] for all detectable isotopes that could be produced, in principle, from muon capture in Double Chooz, and the most likely reaction(s) producing them. Reactions are marked as "exotic" if more than one charged particle or more than two neutrons are emitted, and "obs." if they have been observed prior to this work.

Isotope	Decay mode	Half-life (ms)	Q_β (MeV)	$Q_{\beta n}$	Reaction	Comment
^{6}He	β^-	801	3.505		^{12}C(μ^-, $\nu np\alpha$)^{6}He	Exotic
^{8}He	β^-: 16% βn	119.1	10.664	8.631	^{13}C(μ^-, $\nu p\alpha$)^{8}He	Exotic
^{8}Li	$\beta^-\alpha$	839.9	16.004		^{12}C(μ^-, $\nu\alpha$)^{8}Li	
					^{13}C(μ^-, $\nu n\alpha$)^{8}Li	
^{9}Li	β^-: 50.8% βn	178.3	13.606	11.942	^{13}C(μ^-, $\nu\alpha$)^{9}Li	
^{11}Li	β^-: 83% βn	8.75	20.551	20.049	^{13}C(μ^-, $\nu 2p$)^{11}Li	Exotic
^{11}Be	β^-	13 810	11.509		^{12}C(μ^-, νp)^{11}Be	
^{12}Be	β^-	21.49	11.708		^{13}C(μ^-, νp)^{12}Be	
^{14}Be	β^-: 81% βn	4.35	16.29	15.32	^{18}O(μ^-, $\nu n3p$)^{14}Be	Exotic
^{8}B	$\beta^+\alpha$	770	16.958		^{12}C(μ^-, $\nu 4n$)^{8}B	Exotic
^{12}B	β^-	20.20	13.369		^{12}C(μ^-, ν)^{12}B	Obs.
					^{13}C(μ^-, νn)^{12}B	
^{13}B	β^-: 0.29% βn	17.33	13.437	8.491	^{13}C(μ^-, ν)^{13}B	
^{14}B	β^-	12.5	20.644		^{16}O(μ^-, $\nu 2p$)^{14}B	Exotic
^{15}B	β^-: 93.6% βn	9.93	19.085	17.867	^{18}O(μ^-, $\nu n2p$)^{15}B	Exotic
^{9}C	$\beta^+ p\alpha$	126.5	15.473		^{14}N(μ^-, $\nu 5n$)^{9}C	Exotic
^{15}C	β^-	2449	9.772		^{16}O(μ^-, νp)^{15}C	Exotic
^{16}C	β^-: 99% βn	747	8.010	5.521	^{18}O(μ^-, νnp)^{16}C	
^{17}C	β^-: 32% βn	193	13.161	7.276	^{18}O(μ^-, νp)^{17}C	
^{12}N	β^+	11.000	16.316		^{16}O(μ^-, $\nu 4n$)^{12}N	
^{16}N	β^-	7130	10.421		^{16}O(μ^-, ν)^{16}N	Obs.
^{17}N	β^-: 95.1% βn	4173	8.679	4.536	^{18}O(μ^-, νn)^{17}N	
^{18}N	β^-	620	13.896		^{18}O(μ^-, ν)^{18}N	

nuclear capture rate on ^{13}C is a few percent lower than that of ^{12}C [1]. Because the individual relative errors are 0.01%, these values can be treated as exact for our purposes. Even the difference in ^{13}C fractions in the two scintillators is only 0.17% relative. The most precise measurement reported in this paper has a statistical error over 1% relative, so the neutrino target/γ catcher difference can be neglected and a mass-weighted average value of 1.0919% used instead, again treated as exact. Overall, it is expected that (1.01 ± 0.06)% of the nuclear captures on carbon are on ^{13}C.

C. About oxygen and nitrogen

Both the γ catcher and neutrino target scintillators contain nitrogen and oxygen due to their PPO ($C_{15}H_{11}NO$) component. The neutrino target scintillator additionally has oxygen in the gadolinium complex ($GdO_6C_{33}H_{57}$) and in tetrahydrofuran (C_4H_8O) [8,9]. The acrylic ($C_5H_8O_2$) vessels also contribute oxygen.

The vast majority of the oxygen is in the acrylic vessels. The neutrino target vessel, including supports and stiffeners, contributes 138 kg of oxygen, while the γ catcher vessel contributes 260 kg. Since the acrylic is thin, most decays in it should be observable with only a minor loss in visible energy, with the exception of those in the γ catcher vessel that escape into the buffer. The neutrino target scintillator has an additional 21 kg of oxygen, and the γ catcher scintillator has 3 kg.

After deriving the rate of nuclear captures on carbon in Sec. IV, these figures will be used to derive an estimate for the number of nuclear captures on oxygen. One major difficulty arises. While the nuclear capture probability given a μ^- bound to an oxygen nucleus is well measured, the rate of atomic capture is uncertain. As discussed in [1], there is no good rule for what happens in mixed targets. A large systematic error is taken for this uncertainty in Sec. V.

Nitrogen is only present in the scintillators, with 4.8 kg in the neutrino target and 2.8 kg in the γ catcher. A similar difficulty with regard to the atomic capture probability exists with nitrogen as with oxygen. Given the small total amount of nitrogen, only ^{14}N is important, the contribution of ^{15}N being completely negligible.

Muons may also capture on gadolinium in the neutrino target scintillator, or the various components of steel in the calibration system and phototubes. However, despite the higher probabilities of nuclear capture when μ^- become bound to these atoms, 96.3% in the case of gadolinium [10], the total amounts available are sufficiently small that these elements can be ignored both as possible opportunities for measurement and as sources of background for the measurements presented here.

III. RATE OF STOPPING μ^-

The analyses below determine the number of decay events for various isotopes. To translate these counts to probabilities, one needs to know the number of nuclear μ^- captures. This number is obtained by counting reconstructed stopping muons and using a Monte Carlo simulation to get the μ^-/μ^+ ratio, giving the number of stopping μ^-. Using previous

experimental data, this can be translated into the number of nuclear μ^- captures.

Double Chooz has no capability to distinguish between μ^+ and μ^- tracks. From studies using the MUSIC [11] Monte Carlo simulation along with charge ratio data from MINOS [12,13] and L3+C [14], it is estimated that $(44.1 \pm 0.3)\%$ of stopping muons are μ^-, which gives a 0.7% normalization error for all measurements herein. Results from MUSIC were cross-checked using a custom fast Monte Carlo simulation incorporating the Gaisser model [15], as modified by Guan *et al.* [16]. The error is dominated by the systematic error from L3+C, with only a small contribution resulting from the modeling of our overburden.

Muons that stop in the inner detector scintillator can be identified by selecting events with a large energy deposition in the inner detector and energy in the inner veto consistent with a single muon crossing. By reconstructing candidates under both stopping and through-going hypotheses and selecting based on the relative goodness of fit, an 80% pure sample of muons with stopping points in the neutrino target or γ catcher can be obtained. The remaining 20% are primarily muons that stop in the buffer and through-going muons that pass through inefficient regions of the inner veto. Because of Double Chooz's underground location, the level of contamination by stopping pions is negligible. The muon reconstruction algorithm has been described in detail in Ref. [17]. The position resolution for the stopping point is typically 150 mm in each of x, y, and z.

In order to select a high-purity sample of stopping muons, a series of further selection cuts is used. In particular, candidate muons must have reconstructed stopping points far from the bottom and sides of the γ catcher since many muons reconstructed to stop in these regions are in fact through-going. The stopping position must have $z > -1.175$ m and $r < 1.05$ m, where (0,0,0) is the center of the neutrino target. Further, the energy deposition in the inner veto must be within a tight range consistent with the reconstructed crossing, and the reduced χ^2 of the muon track fit must be less than 2.0. Finally, stopping muon candidates are rejected if another muon event precedes them by less than 0.5 ms. This ensures that any neutrons produced can be assigned to the correct muon.

It was found that $(99.72 \pm 0.19)\%$ of muons passing these cuts were stopping muons. This was determined by testing the uniformity of the probability of a Michel decay following a stopping muon candidate across the selected spatial region. It was cross-checked, at lower precision, by verifying that the total number of observed Michel decays over 10 MeV was consistent with the selected stopping muon count. Efficiencies for this study were evaluated using the Michel spectra for μ^- bound to carbon [18] and free μ^+ [19]. A second cross-check verified the spatial uniformity of the probability of observing a ^{12}B decay after a stopping muon candidate.

To test the rate of reconstruction failures directly, a sample of through-going muon events from our data set was modified to remove inner veto hits at the endpoint. This causes them to resemble muons that stop in the buffer, allowing us to test the rate at which such muons reconstruct with end points far from the edge. No such reconstructions were found, and a limit was set that less than 0.03% of the selected sample consists of such misreconstructions. Because our technique of hit removal is only an approximation for the real background, this study is treated as a cross-check for numerical purposes, but gives us confidence that the purity quoted above is conservative.

In this high purity sample, there are 1 628 874 reconstructed stopping muons. Of the μ^-, $(99.8 \pm 0.1)\%$ become bound in carbon atoms. The uncertainty on this number derives from the uncertainty on the probability of a muon becoming attached to noncarbon atoms, as described in Sec. II C. From the purity and μ^- fractions above, this gives $(7.149 \pm 0.054) \times 10^5$ μ^- that are available to undergo nuclear capture on carbon. Given total nuclear capture probabilities of $(7.69 \pm 0.09)\%$ and $(7.3 \pm 0.4)\%$ for ^{12}C and ^{13}C [1], respectively, and 489.5 days of lifetime, the nuclear capture rates in the high purity sample are 111.1 ± 0.6/day for ^{12}C and 1.16 ± 0.06/day for ^{13}C.

IV. ^{12}B/^{13}B ANALYSIS

Previous experiments have measured ^{12}B production by stopping muons in carbon, although none have done so using a method that can separate production by ^{12}C and ^{13}C [1,20]. Given its short half-life and high Q_β value of (see Table II), ^{12}B is readily observable. This applies to ^{13}B as well, but is quite difficult to distinguish from ^{12}B given its very similar half-life and β spectrum.

Selection

β decay candidates must occur at least 1 ms after a stopping muon without a Michel electron. The efficiency for observing Michel decays is about 78%, as determined by comparing the number found in the high purity sample of stopping muons to the number expected given the muon charge ratio and inclusive capture probability. The stopping muon must be followed by at least 100 s of continuous data taking.

An event is selected as a β decay if it is not light noise (spontaneous emission of light from PMTs, described in [4]) and is between 4 and 15 MeV. The energy cut has an efficiency of $(85.0 \pm 0.7)\%$, as found from a low-background subset of ^{12}B events. In evaluating this efficiency, the portion of the ^{12}B spectrum below 0.5 MeV was filled with a β spectrum [21–27] Monte Carlo simulation, taking into account the detector response. In addition, it must not occur within 0.5 ms after any subsequent muon, to avoid selecting neutron captures as β decays.

The overall selection efficiency, including inefficiency due to light noise removal, the ^{12}B energy cut, Michel electron selection, subsequent muon veto, and the requirement of continuous data taking, is $(81.0 \pm 0.6)\%$. No position cut is made for the β decay in order to avoid incurring additional error due to the efficiency of such a cut. While this is advantageous for the measurement of ^{12}B, a position cut will be used in the following sections for all other isotope searches to reduce background.

This sample of events is divided into those in which the muon is followed by zero, one, or two neutron captures. In the zero neutron case, the signal is either $^{12}\mathrm{C}(\mu^-,\nu)^{12}\mathrm{B}$ or $^{13}\mathrm{C}(\mu^-,\nu)^{13}\mathrm{B}$. In the one neutron case, the signal is $^{13}\mathrm{C}(\mu^-,\nu n)^{12}\mathrm{B}$. The two neutron case exists to account for

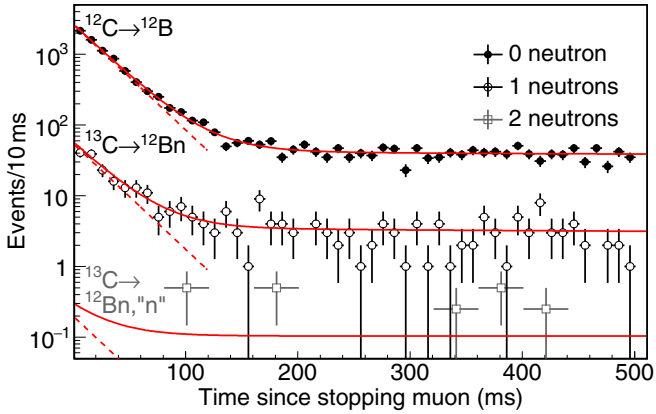

FIG. 1. ^{12}B production with and without a neutron, interpreted as ^{13}C$(\mu^-,\nu)^{12}$B (filled circles), ^{13}C$(\mu^-,\nu n)^{12}$B (open circles). Neutron efficiency and accidental neutronlike events are accounted for, including those occurring along with a real neutron (open squares; "n" denotes an accidental neutronlike event). The solid red curves show the fit results, while the dashed red lines give the ^{12}B components thereof.

this reaction when an additional accidental neutronlike event is selected, which has a probability of 1.1×10^{-4}. The neutron efficiency during the data taking period analyzed here is a function of the preceding muon energy and has a value, averaged over the neutrino target and γ catcher, of $(57 \pm 1)\%$.

An extended unbinned maximum likelihood [28] fit using the event timing is done simultaneously for these three reactions. The fit takes into account neutron efficiencies on an event-by-event basis, with nuisance parameters for production of ^{8}Li [half-life (839.9 ± 0.9) ms], ^{8}Li $+n$, ^{9}Li [half-life (178.3 ± 0.4) ms], ^{9}Li $+n$, ^{16}N [half-life (7.13 ± 0.02) s], and accidental coincidences. The lifetimes of each isotope are allowed to float with pull terms constraining them within published errors. The total probability of isotope production from ^{13}C is constrained to be at most 100% with a pull term taking into account the error on the total nuclear capture rate on ^{13}C. The neutron efficiency is included as a fit parameter and allowed to float within its errors.

Selected events and the fits are shown in Fig. 1. The results of the fit for each reaction follow. For each, three numbers are given: (1) the probability per atomic capture, which has the least dependence on external measurements, (2) the capture rate, which relies on previous measurements of the bound μ^- lifetime, (2028 ± 2) ns for ^{12}C and (2037 ± 8) ns for ^{13}C [1], and (3) the probability per nuclear capture, which depends on the total nuclear capture probability. The total nuclear capture probability has been determined using the bound μ^- lifetime, so the external uncertainties on the capture rate and nuclear capture probability have the same origin. However, since determining the nuclear capture probability involves subtracting two similar numbers, $P = (\tau_{\text{free}} - \tau_{\text{bound}})/\tau_{\text{free}}$, the fractional uncertainty is much larger.

Results are given in Table III. All sources of errors handled in the fit, such as the neutron efficiency and external lifetime measurements, are considered statistical. Note the asymmetric errors for ^{12}C$(\mu^-,\nu)^{12}$B. These are due to the possibility of a large contribution from ^{13}B. Since the best fit for ^{13}B is zero, this source of error is one-sided.

TABLE III. Results for ^{12}B and ^{13}C production from carbon, expressed as a probability per atomic capture (top), per nuclear capture (middle) and as a transition rate (bottom). In each case, the total error is given, and then each component of the error is shown. N_{μ^-} gives the error due to μ^- counting, P(cap) is the error due to knowledge of the total nuclear capture rate, and τ_{μ^-} is the error due to the knowledge of the bound μ^- lifetime. Limits are given at 90% CL.

Probability per atomic capture (%)

Reaction	Prob., total error	Stat	N_{μ^-}	^{12}B eff.
^{12}C → ^{12}B	$1.322^{+0.022}_{-0.042}$	$^{+0.016}_{-0.040}$	±0.010	±0.010
^{13}C → ^{12}Bn	3.75 ± 0.36	±0.36	±0.03	±0.03
^{13}C → ^{13}B	<2.8			

Probability per nuclear capture (%)

Reaction	Prob., total error	Stat	N_{μ^-}	^{12}B eff.	P(cap)
^{12}C → ^{12}B	$17.35^{+0.35}_{-0.59}$	$^{+0.21}_{-0.52}$	±0.13	±0.13	±0.21
^{13}C → ^{12}Bn	51.6 ± 5.6	±5.0	±0.4	±0.4	±2.6
^{13}C → ^{13}B	<40				

Capture rate ($\times 10^3$ s^{-1})

Reaction	Rate, total error	Stat	N_{μ^-}	^{12}B eff.	τ_{μ^-}
^{12}C → ^{12}B	$6.57^{+0.11}_{-0.21}$	$^{+0.08}_{-0.20}$	±0.05	±0.05	±0.01
^{13}C → ^{12}Bn	18.4 ± 1.8	±1.8	±0.1	±0.1	±0.1
^{13}C → ^{13}B	<14				

The most recent previous measurement of any of these processes comes from Ref. [20], in which the probability per atomic capture for ^{12}C → ^{12}B is given as $(1.55 \pm 0.06)\%$. This was converted by Ref. [29] to a rate of $(7.05 \pm 0.27) \times 10^3$ s^{-1} and subsequently quoted by Ref. [1] as a probability per nuclear capture of $(18.6 \pm 0.7)\%$. Two corrections to these figures are needed. From the beginning, the contributions from ^{13}C are neglected, which requires a downward correction. Second, the rate results from an erroneous division of the atomic capture probability by the free muon lifetime, rather than the bound lifetime. This requires an upward correction. Our best estimates of the correct figures for comparison are $(1.51 \pm 0.07)\%$ for the probability per atomic capture, $(19.6 \pm 0.8)\%$ per nuclear capture, and $(7.44 \pm 0.35) \times 10^3$ s^{-1} for the rate. In all cases, our figures are about 2.5σ lower.

V. TOTAL NUCLEAR CAPTURE RATES

For all remaining reactions, a looser selection is used for stopping muons to increase the statistics for processes less common than ^{12}B production. This selection relaxes the above-described requirements on stopping position, track fit quality, and inner veto energy. Stopping muon candidates are accepted if the stopping point is not within 35 mm of the bottom or sides of the γ catcher and if the fit reduced χ^2 is less than 10. The constraints on acceptable inner veto energy are also loosened.

To determine the number of true stopping μ^- in this expanded sample, the ratio of ^{12}B-like events found in the two

samples is used. The high-purity sample has 7882 ± 95, while $17\,580 \pm 150$ additional events are found in the expanded sample. This gives $(2.309 \pm 0.032) \times 10^6$ atomic captures on carbon in the new sample. Some impurity and a larger normalization error are therefore traded for 3.2 times the statistics.

The two samples have very similar $^{12}C/^{13}C$ ratios, as described in Sec. II B, however the new sample contains substantially more oxygen by including the neutrino target vessel and supports. There is therefore a concern that the simple ratio above may be incorrect due to the presence of ^{12}B from the reaction $^{16}O(\mu^-,\nu\alpha)^{12}B$. Data on this reaction appear to be limited to a single emulsion experiment [30], but even under moderately pessimistic assumptions, this is enough to argue that it has a negligible effect.

The following rates for the expanded sample are found using the total number of atomic captures for carbon above and the known total nuclear capture probability:

(i) ^{12}C;
(a) 4664 ± 65 atomic captures/day;
(b) 358.8 ± 6.5 nuclear captures/day;
(ii) ^{13}C;
(a) 51.5 ± 0.71 atomic captures/day;
(b) 3.75 ± 0.19 nuclear captures/day.

The error on the ^{12}C nuclear capture rate is shared equally between the ^{12}B-like event statistics discussed above and the probability of nuclear capture following atomic capture. The error on ^{13}C results mainly from the probability of nuclear capture.

Rates for other isotopes are estimated using the chemical composition of the detector. These are given as ranges to emphasize the large uncertainties surrounding probability of atomic capture in chemical compounds. Based on data presented in Ref. [1], it is conservatively assumed that oxygen (nitrogen) overcaptures by a factor of 1–2 (1–1.5) as compared to its number density. The probability within these ranges will be treated as uniform:

(a) 0.2–0.3 ^{14}N nuclear captures/day;
(b) 6–13 ^{16}O nuclear captures/day;
(c) 1–2 ^{17}O nuclear captures for the entire data set;
(d) 5–12 ^{18}O nuclear captures for the entire data set.

VI. βn ISOTOPES

The Double Chooz detector is optimized for the detection of $\bar{\nu}_e$ via the inverse β decay reaction, $p(\bar{\nu}_e,e^+)n$. The resulting positron gives a prompt signal and the subsequent capture of the neutron on either gadolinium or hydrogen gives a delayed coincidence. A major background to this process is the production of ^9Li by cosmic muons, as its βn decay produces a signal that is nearly indistinguishable from the inverse β decay signal. For this analysis, the existing inverse β decay selection is used to select βn decays in the neutrino target and γ catcher, both for events with captures on gadolinium [4] and hydrogen [31].

An excess over background of βn events is found near stopping muons both in time and space. Events for which the reconstructed distance from the muon stopping point to the β decay is less than 300 mm are selected for the fit described below. The efficiency of this cut is estimated using the sample of ^{12}B events (see Sec. IV) and is found to be $(92.0 \pm 0.5)\%$ in the neutrino target and $(74.9 \pm 0.5)\%$ in the γ catcher (see Fig. 2). Fifteen βn-like events are selected within 300 mm and 400 ms of stopping muons. The spatial distribution for these events is shown in Fig. 3. The close correlation in space demonstrates that the isotopes are being produced at the stopping point, rather than along the muon track. This also excludes the possibility that they are created by correlated through-going muons.

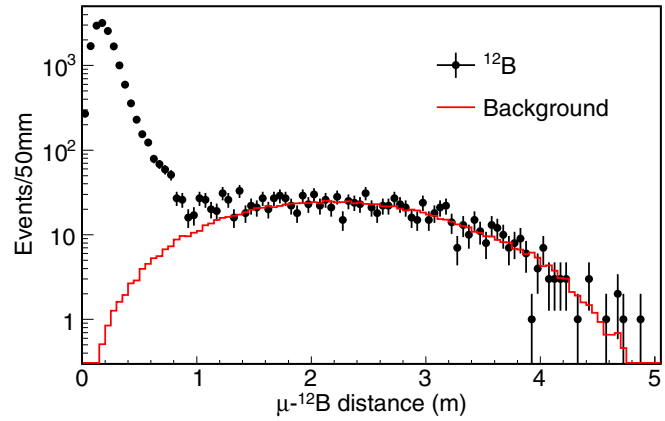

FIG. 2. Distance between selected ^{12}B events and preceding stopped muon (black), as compared to a background sample (red). The efficiency for a distance cut is the fraction of background-subtracted ^{12}B within the cut.

The time distributions are shown in Fig. 4 for the case in which no requirement is put on neutron detection following the muon and the case of selecting one neutron following the muon. The flat background is formed from accidental coincidences between stopping muon candidates and βn-like events. It is due almost entirely to reactor neutrino interactions. As at least one reactor of the Chooz power plant was active for 98% of this data set's lifetime, this background is unavoidable. The efficiency of this selection for ^9Li βn decays in the neutrino target with the neutron capturing on gadolinium is

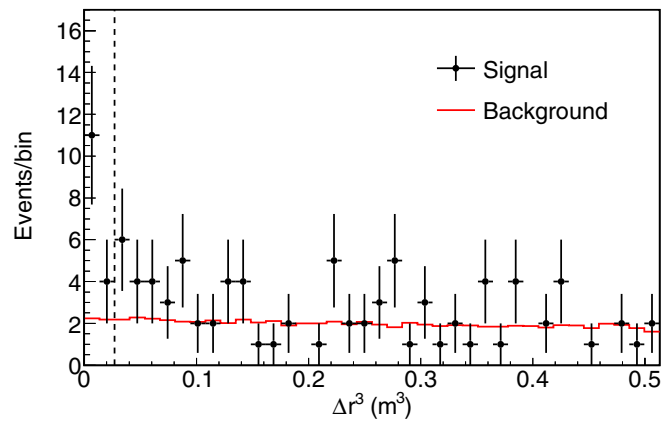

FIG. 3. The distance-cubed distribution of βn events less than 0.4 s after a stopping muon with all other cuts applied. The dashed line is the Δr cut.

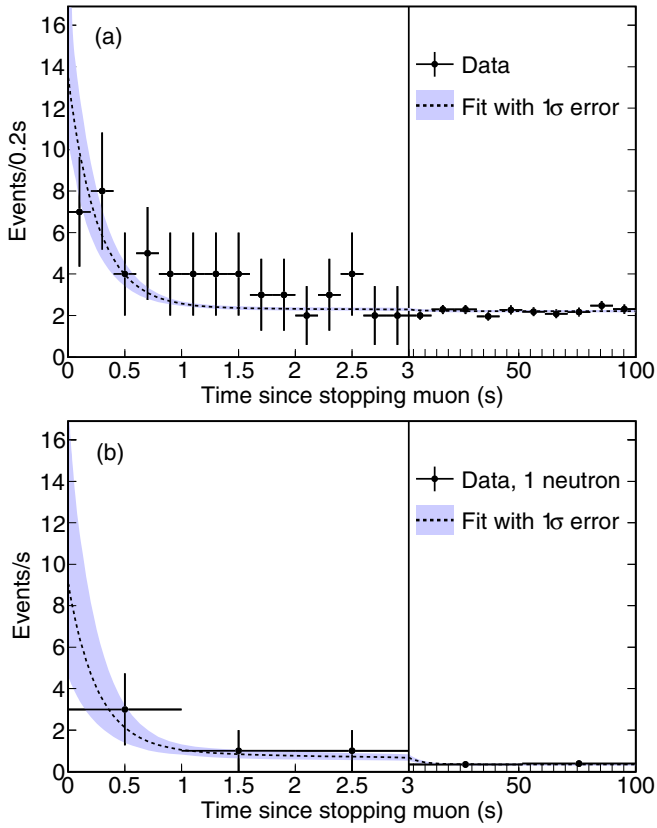

FIG. 4. Observation of $^{nat}C(\mu^-,\nu X)^9Li$. (a) With no requirement for a neutron following the muon. (b) Requiring exactly one neutron. The fit results for ^{9}Li plus correlated (^{16}C, ^{17}N) and accidental ($\bar{\nu}_e$) backgrounds are shown. Note the change of horizontal scale at 3 s.

$(82.0 \pm 0.5)\%$ and for decays in the γ catcher with the neutron capturing on hydrogen is $(62.7 \pm 0.4)\%$.

In the case of no neutron requirement, the time distribution is fit using the unbinned maximum likelihood method [28] under the hypothesis that the excess over a flat background consists of a combination of several βn isotopes (half-lives given in parentheses): ^{11}Li (8.75 ms), ^{13}B (17.33 ms), ^{8}He (119.1 ms), ^{9}Li (178.3 ms), ^{16}C (747 ms), and ^{17}N (4.183 s). The fit is done in three bins of reactor power to take advantage of the lower background rates during zero- and one-reactor periods. Some potentially present βn isotopes were excluded from the fit. First, ^{14}Be, ^{15}B, and ^{12}Be were excluded because their half-lives of 4.35, 9.93, and 22 ms are close to those of ^{11}Li and ^{13}B, and, as will be shown in Sec. VI, there is no evidence of an O (10 ms) component. Second, ^{17}C was excluded because its half-life of 193 ms is very close to ^{9}Li's and it can only be produced by $^{18}O(\mu^-,\nu p)^{17}C$. With a βn branching ratio of 32%, it is expected to contribute much less than one event for any reasonable estimate of the $(\mu^-,\nu p)$ probability. Third, ^{18}N is excluded because its half-life of 620 ms is very close to ^{16}C's and with a βn branching ratio of only 7%, the expected number of events is less than 1 regardless of the probability of $^{18}O(\mu^-,\nu)^{18}N$.

With all six isotopes free in the fit, there is a 5.5σ preference for a βn signal over the background-only hypothesis. The fit is unable to constrain the probabilities of producing the

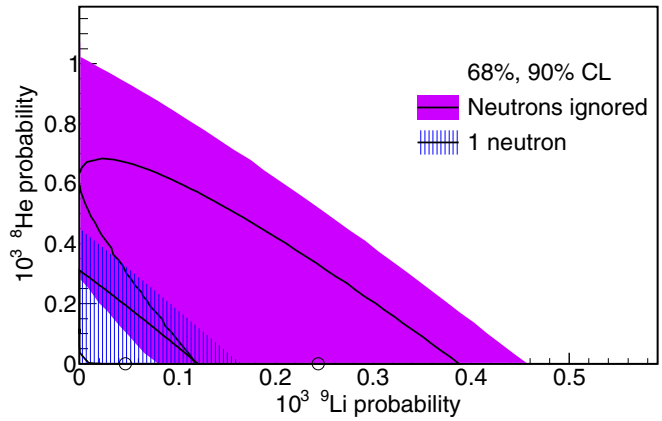

FIG. 5. 90% and 68% contours for ^{9}Li and ^{8}He with no neutron requirement (violet) and requiring a neutron (blue), with probabilities given per ^{nat}C capture.

isotopes with half-lives longer than ^{9}Li's due to the amount of accidental background. With all isotopes free to take any value in the fit, significant degeneracy exists between these and the shorter lived isotopes. In order to be able to measure the ^{9}Li and ^{8}He probabilities, the contributions from ^{16}C and ^{17}N are therefore given pull terms constraining their probabilities to $(5 \pm 5)\%$ and $(50 \pm 25)\%$, respectively, based on previous measurements of similar reactions in other isotopes [1,5]. This done, the significance of ^{9}Li and ^{8}He specifically being present is 2.7σ. As shown in Fig. 5, there is little power to distinguish these two isotopes from each other.

As shown in Fig. 6 the β spectrum of selected βn events is compatible with that of ^{9}Li plus the reactor neutrino background. While the statistics do not allow a detailed fit, the event at 9.47 MeV provides further evidence against the hypothesis that neutrinos or other backgrounds are the only events present, since only a very small fraction of reactor neutrinos reach this energy, and the rate of other neutrino backgrounds is small compared to the neutrino rate. It is also

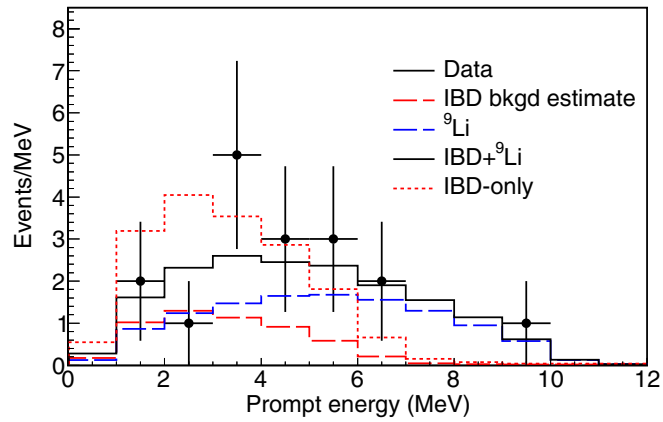

FIG. 6. Prompt energy for ^{9}Li candidates with $\Delta t < 0.5$ s. An IBD background estimate from off-time samples is shown in dashed red. MC for ^{9}Li is shown in dashed blue, normalized so that the sum (solid black) matches the data. In dashed red is shown the IBD-only spectrum normalized to the data. The highest energy event has 9.47 MeV.

incompatible with all events being ^{8}He, ^{16}C, ^{17}C, or ^{17}N (see βn endpoint in Table I).

Assuming no ^{8}He, the probability of forming ^{9}Li from a muon capture in $^{\rm nat}$C is found to be $[2.4 \pm 0.9(\text{stat}) \pm 0.04(\text{syst})] \times 10^{-4}$. The systematic error is dominated by the uncertainty on the number of μ^- captures. If no constraint is put on ^{8}He, only limits can be set on it and ^{9}Li. The ^{9}Li limit with ^{8}He unconstrained is $<4 \times 10^{-4}$ at 90% CL. For ^{8}He it is $<7 \times 10^{-4}$ at 90% CL.

If ^{9}Li were produced via $^{12}\text{C}(\mu^-,\nu n2p)^{9}\text{Li}$, most events would have an observable neutron capture between the stopping muon and the β decay. Because only a minority of stopping muon candidates satisfy this demand, requiring observation of this neutron reduces the neutrino background considerably. Efficiency for observing these neutrons is reduced by deadtime following muons during the data period used in this paper; it is 57% for the neutrino target and 87% for the γ catcher.

In fact, few of the events survive the neutron requirement, as shown in Fig. 4. The remaining events give an overall significance of βn production of 3.4σ and are compatible with the expected rate of $^{18}\text{O}(\mu^-,\nu n)^{17}\text{N}$. The fitted amount of ^{9}Li + ^{8}He in the two samples is incompatible with the hypothesis of $^{12}\text{C}(\mu^-,\nu n2p)^{9}\text{Li}$ at the 2.7σ level, indicating that the reaction $^{13}\text{C}(\mu^-,\nu\alpha)^{9}\text{Li}$ most likely is responsible for the ^{9}Li produced by stopping muons. Under this interpretation, and assuming no ^{8}He production, the probability for production from ^{13}C is $[2.4 \pm 0.9(\text{stat}) \pm 0.05(\text{syst})]\%$.

^{11}Li and ^{13}B

The above analysis also constrains ^{11}Li and ^{13}B, which would appear as early βn events given their half-lives of 8.75 and 17.33 ms, respectively. Both would be produced from ^{13}C without neutrons. The constraint on ^{13}B is independent of that found in Sec. IV, since in that fit the β mode was used.

The efficiency for selecting ^{11}Li is reduced to 92.7% compared to ^{9}Li due to events lost in the 1-ms muon veto. The fraction of ^{11}Li that undergoes βn decay is 83%. The efficiency for selecting ^{13}B is likewise 96.1% relative to ^{9}Li. Its βn branching fraction is only 0.29%.

The procedure described in the previous section is repeated, but requiring no neutrons. The fit finds no evidence for either isotope (see Fig. 7). Because of the low probability of ^{13}B -βn, this fit adds no significant information to the result of the ^{12}B /^{13}B fit described in previous sections. The ^{11}Li probability, allowing the ^{13}B contribution to float freely, is $<0.7\%$ at 90% CL.

VII. DECAY CHAIN: ^{12}Be

The isotope ^{12}Be is a special case because it decays via a two-step chain to ^{12}C via ^{12}B. The two β decays are very similar in energy and lifetime. The first decay ($^{12}\text{Be} \rightarrow {}^{12}\text{B}$, half-life 21.49 ms, β endpoint 11.7 MeV) is selected with a similar procedure as used to find ^{12}B in Sec. IV. The decay is required to occur 1–100 ms after the stopping muon (92.9% efficiency, using the ^{12}Be lifetime), within 400 mm of its stopping point (91.6% efficiency, as judged by the sample of ^{12}B decays, as in Sec. VI), and have energy 3–12 MeV

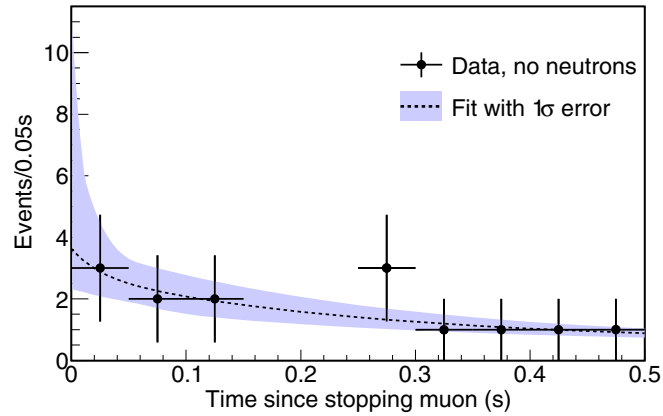

FIG. 7. Search for ^{11}Li and the βn mode of ^{13}B. The dashed line shows the best fit, which finds no significant amount of ^{11}Li or ^{13}B.

(89 ± 2% efficiency, based on Monte Carlo simulation). The overall selection efficiency for the ^{12}Be decay is (75 ± 2)%.

If a ^{12}Be candidate is found, the selection is then repeated to search for the ^{12}B decay. The distance cut is applied relative to the ^{12}Be decay candidate, since the position reconstruction for pointlike events has higher resolution than that for muons. The ^{12}B decay is required to occur 1–150 ms after the ^{12}Be decay (96.0% efficiency), within 400 mm (97% efficiency), and have energy 3–15 MeV (92.5 ± 0.7% efficiency). The ^{12}Be and ^{12}B decays are not allowed to occur within 1 ms of each other to avoid selection of inverse β decay events or ^{12}B produced by neutron spallation. The overall selection efficiency for the ^{12}B is (85 ± 1)%. The selection efficiency for the decay chain is (63 ± 2)%.

No events are selected. An upper limit is set of $< 0.20\%$ per ^{13}C capture at 90% CL.

VIII. β ISOTOPES

A. ^{8}Li

For ^{8}Li, for which the signal is a single β decay (half-life 839.9 ms, β endpoint ∼13 MeV), the same analysis as was used to measure ^{12}B in Sec. IV is used, but with modifications to reduce background. The ^{8}Li decay is required to have an energy of 5–14 MeV and be within 400 mm of the stopping muon. Events are selected with and without neutrons following the muon. Events with a neutron are interpreted as $^{13}\text{C}(\mu^-,\nu n\alpha)^{8}\text{Li}$ and those without as $^{12}\text{C}(\mu^-,\nu\alpha)^{8}\text{Li}$.

Since the ^{8}Li lifetime is fairly close to the ^{9}Li lifetime, inverse β decay candidates are excluded from the sample to reduce contamination from ^{9}Li. The remaining 49.2% of ^{9}Li that undergo plain β decay are not affected by this cut. The small amount of remaining ^{9}Li is constrained with pull terms derived from the βn analysis.

To suppress background caused by muon-induced $^{12}\text{C}(n,p)^{12}\text{B}$, a likelihood classifier is used that takes as input the distance between a candidate decay and the most recent through-going muon and the number of neutron captures following that muon [4]. This classifier removes 50% of the accidental background and has a signal efficiency of 90.6%.

The selected events and fit results are shown in Fig. 8. If the ^{8}Li half-life is allowed to float without a pull term in

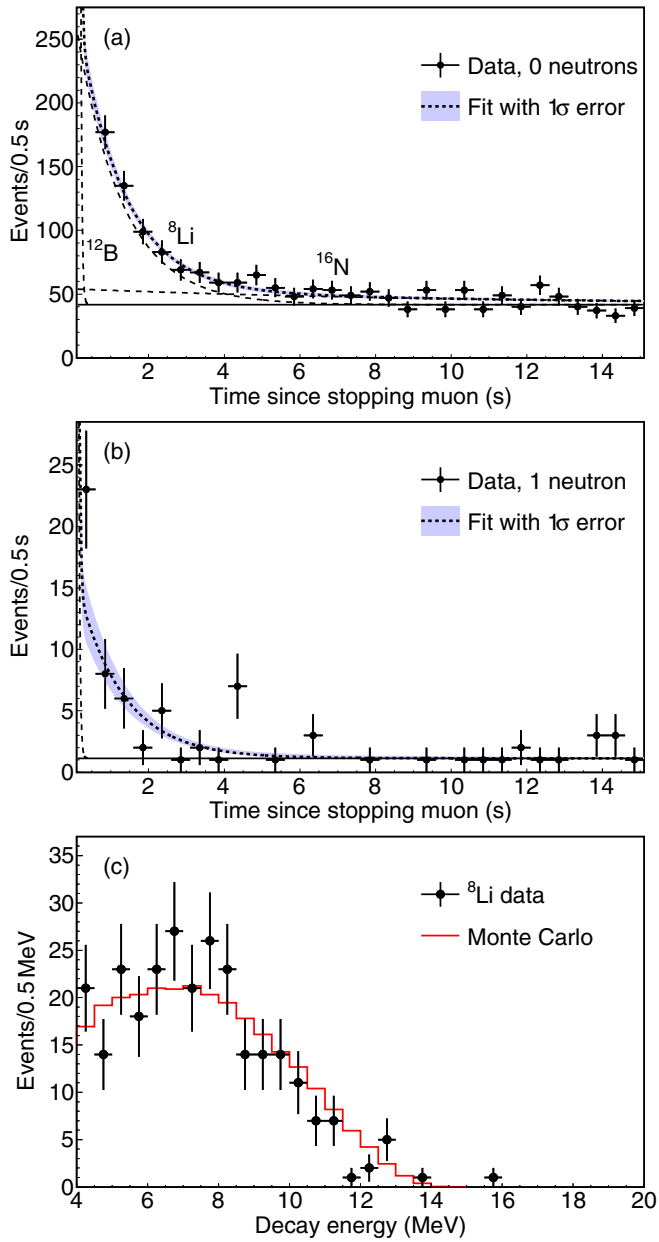

FIG. 8. ^{8}Li search. (a) Joint fit for ^{12}B, ^{8}Li, ^{16}N, and accidentals when no neutrons follow the muon. (b) Same, with one neutron. (c) Energy of events in the zero-neutron case with a tighter cut of $\Delta r < 200$ mm when 0.3 s $< \Delta t <$ 2 s (points). The solid line shows Monte Carlo normalized to the data.

the zero (one) neutron sample alone, the result is 870^{+120}_{-100} ms (750^{+260}_{-270} ms), as compared to the accepted value of 839.9 ms.

The probability of ^{12}C$(\mu^-,\nu\alpha)^{8}$Li per nuclear capture is found to be $[0.64 \pm 0.04(\text{stat}) \pm 0.02(\text{syst})]\%$, where the systematic error is dominated by the uncertainty on the ^{8}Li energy cut efficiency. The probability of ^{13}C$(\mu^-,\nu\alpha n)^{8}$Li per nuclear capture is found to be $[5.1^{+1.1}_{-1.0}(\text{stat}) \pm 0.3(\text{syst})]\%$, where the systematic error is dominated by the uncertainty on the fraction of muons that undergo nuclear capture on ^{13}C. It should be noted that since Double Chooz is nearly blind to heavy charged particles, these probabilities are not correct if reactions such as ^{12}C$(\mu^-,\nu n^3\text{He})^{8}$Li or ^{12}C$(\mu^-,\nu ndp)^{8}$Li occur at any significant rate.

B. Isotopes produced with many neutrons

The isotopes ^{8}B, ^{12}N, and ^{9}C must be produced via the emission of four or more neutrons by the parent nucleus following muon capture, which allows for a nearly background-free search. First, ^{12}C$(\mu^-,\nu 4n)^{8}$B is considered. The resulting ^{8}B has a half-life of 770 ms and a β^+ endpoint of $\sim$14 MeV (it decays to a broad resonance of ^{8}Be), providing up to 15 MeV of visible energy. The average efficiency for observing all four neutrons is $(48 \pm 2)\%$. Candidate ^{8}B events are selected with 4–18 MeV, which has $(97 \pm 1)\%$ efficiency due to the positron annihilation following the β^+ decay. Candidates are required to be within 400 mm of the stopping muon. These energy and position cuts are shared with the other isotopes in this section. The overall efficiency is $(40 \pm 2)\%$. No events are selected, and a limit of $<3.2 \times 10^{-5}$ per nuclear capture on ^{12}C at 90% CL is set.

Next, ^{16}O$(\mu^-,\nu 4n)^{12}$N is examined. With a β^+ endpoint of 17.3 MeV and half-life of only 11 ms, we restrict the search to 1–100 ms and can allow events with either three or four observed neutrons without admitting significant background. As ^{12}N would be produced primarily in the acrylic, and the neutron efficiency is a function of position, this efficiency is reevaluated and found to be 70% for seeing at least three out of four neutrons. The overall selection efficiency is 54%. No events are selected. A limit is set of $<8 \times 10^{-4}$ per capture on ^{16}O at 90% CL. The systematic error on the number of oxygen captures is taken into account in this limit using the method described in Ref. [32] taking the prior to be flat in the range quoted in Sec. V.

Finally, we search for ^{9}C. Possible production mechanisms include ^{16}O$(\mu^-,\nu p6n)^{9}$C, ^{16}O$(\mu^-,\nu d5n)^{9}$C, and ^{14}N$(\mu^-,\nu 5n)^{9}$C. The half-life of ^{9}C is 127 ms and it has a β^+ endpoint of 15.5 MeV. Events are selected between 1 ms and 1 s if at least four neutrons are observed after the muon. In the case of oxygen, it is conservatively assumed that the true number of neutrons is 5. Given this assumption, the neutron efficiency is 64% for an overall efficiency of 53%. With no signal and no background, a limit of $<9 \times 10^{-4}$ at 90% CL is set. In the case of nitrogen, the neutron efficiency is 63% and overall efficiency is 55%. A limit is set of $<3.6\%$ per nuclear capture on ^{14}N at 90% CL.

C. Long-lived isotopes: ^{15}C and ^{11}Be

The isotopes ^{15}C, ^{16}N, and ^{11}Be are those with the longest half-lives included in this analysis, being 2.449, 7.13, and 13.81 s, respectively. Since the fraction of captures on ^{16}O that produce ^{16}N is already known to be $(11 \pm 1)\%$ [1], it is treated as a background for the other isotopes. It and ^{15}C can be produced by oxygen in the acrylic, while ^{11}Be is produced from carbon, primarily in the scintillator.

Accidental background limits our ability to observe long-lived isotopes. For this search, a very tight spatial cut is made, restricting the decay candidate to be within 200 mm of the muon. Events are vetoed if any neutrons are observed. The

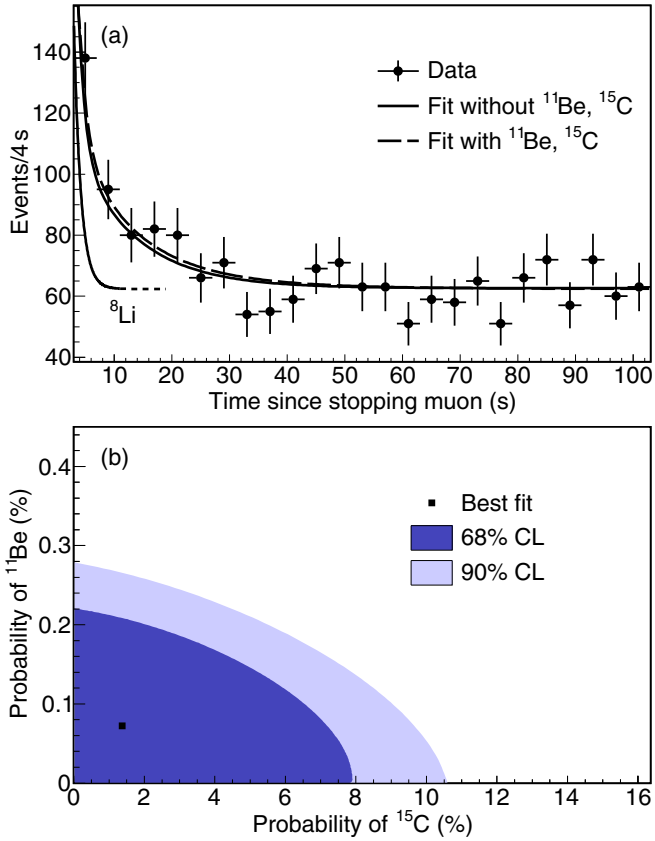

FIG. 9. (a) Search for ^{11}Be and ^{15}C. The solid (dashed) line shows the best fit without (with) ^{11}Be or ^{15}C. The lower curve shows the contribution of ^{8}Li; all contribution from ^{12}B is to the left of the plot area due to its short half-life. (b) Statistics-only confidence regions for ^{15}C and ^{11}Be. Blue (tan) shows 68% (90%) CL.

candidate must be at least 1 ms after the most recent muon anywhere in the detector and at least 0.1 ms after the previous trigger. The ^{12}B likelihood (see Sec. VIII A) is applied. The decay energy is restricted to 4–12 MeV. The efficiencies are 33% for ^{11}Be, 27% for ^{15}C, and 27% for ^{16}N.

A joint fit for ^{12}B, ^{8}Li, ^{15}C, ^{16}N, and ^{11}Be is performed. With all isotopes freely floating, the fit favors the presence of some combination of ^{15}C, ^{16}N, and ^{11}Be, as compared to none, at 6.4σ (see Fig. 9). The fit prefers to explain nearly all of the excess as ^{16}N, finding $7.2^{+1.3}_{-3.4} \times 10^2$ ^{16}N events, corrected for efficiencies, compared to an expectation of (3.0–7.0) $\times 10^2$ given the amount of oxygen in the detector and the known ^{16}N production probability.

To produce the final results for ^{11}Be and ^{15}C, a pull term is used for ^{16}N, constraining it to the expected number of events within errors. No significant amount of the other isotopes is found. Limits are set of $< 0.20\%$ for ^{12}C$(\mu^-,\nu p)^{11}$Be at 90% CL and $< 9\%$ for ^{16}O$(\mu^-,\nu p)^{15}$C at 90% CL.

D. ^{6}He

The half-life of ^{6}He is very close to ^{8}Li's (801 and 840 ms, respectively), but it has a much lower β endpoint of 3.51 MeV. When fitting for ^{8}Li above, any possible contribution from ^{6}He is removed by the energy cut. To search for ^{6}He, however, it is necessary to fit the spectrum, setting this analysis apart from all others reported on in this paper.

To search for a correlation between low energy ^{6}He decays and their parent muons, a complex fit is needed to reduce the accidental background. Most of this background results from γ decays outside the γ catcher, such as in the PMTs and surrounding rock, and so drops dramatically as one moves towards the center of the neutrino target. Therefore, a binned fit is done in energy and position. There are five spatial bins, the first four of which have approximately equal volume:

(1) $r < 740$ mm and $|z| < 740$ mm (2.546 m^3), where r is horizontal distance from the center of the neutrino target and z is the vertical distance;

(2) $r < 933$ mm and $|z| < 933$ mm, excluding the innermost volume (2.557 m^3);

(3) $r < 1068$ mm and $|z| < 1068$ mm, excluding the innermost two volumes (2.551 m^3);

(4) $r > 1068$ mm or $|z| > 1068$ mm and inside the neutrino target (2.759 m^3);

(5) in the γ catcher (22.74 m^3).

Each spatial bin is binned in energy with 0.125-MeV bins in the range 0.375–15 MeV. The following selection is used: The time since the stopping muon must be at least 0.3 s and not more than 1.602 s (two ^{6}He half-lives). The lower bound reduces the background from correlated ^{12}B to 1.1 events for the whole data set. The decay must be within 200 mm of the muon stopping point, at least 0.1 ms since the last trigger, at least 1 ms since the last muon, and must not have a high likelihood of being ^{12}B produced by a through-going muon. In four separate analyses, the muon must be followed by exactly 0, 1, 2, or 3 neutrons.

The ^{6}He efficiency after these cuts ranges from 25% for the zero-neutron case to 10% for the three-neutron case. The fit is done with 16 free parameters:

(1) The amount of ^{6}He.

(5) The accidental background normalization in each region. This background is measured using an off-time window. The normalization is constrained by a pull term to be within the statistical errors of the off-time sample.

(5) The amount of ^{8}Li in each region, which is the dominant background at the ^{6}He endpoint for the inner regions.

(5) The amount of ^{16}N in each region. This is allowed to float freely in each region since its 6.1-MeV γ means that the number reconstructed in each region is not simply the fraction produced there. The inclusion of ^{16}N is not very important, but accounts for the 6–7-MeV peak seen in the plots and avoids slightly overestimating the ^{8}Li background in the signal region.

TABLE IV. Results for ^{6}He search with various neutron requirements.

N_n	Signif.	Limit	Value
0	0.5σ	$<0.43\%$	
1	2.7σ	$<0.47\%$	$[0.33^{+0.14}_{-0.13}(\text{stat}) \pm 0.02(\text{syst})]\%$
2	0.5σ	$<7 \times 10^{-4}$	
3	0.2σ	$<8 \times 10^{-4}$	

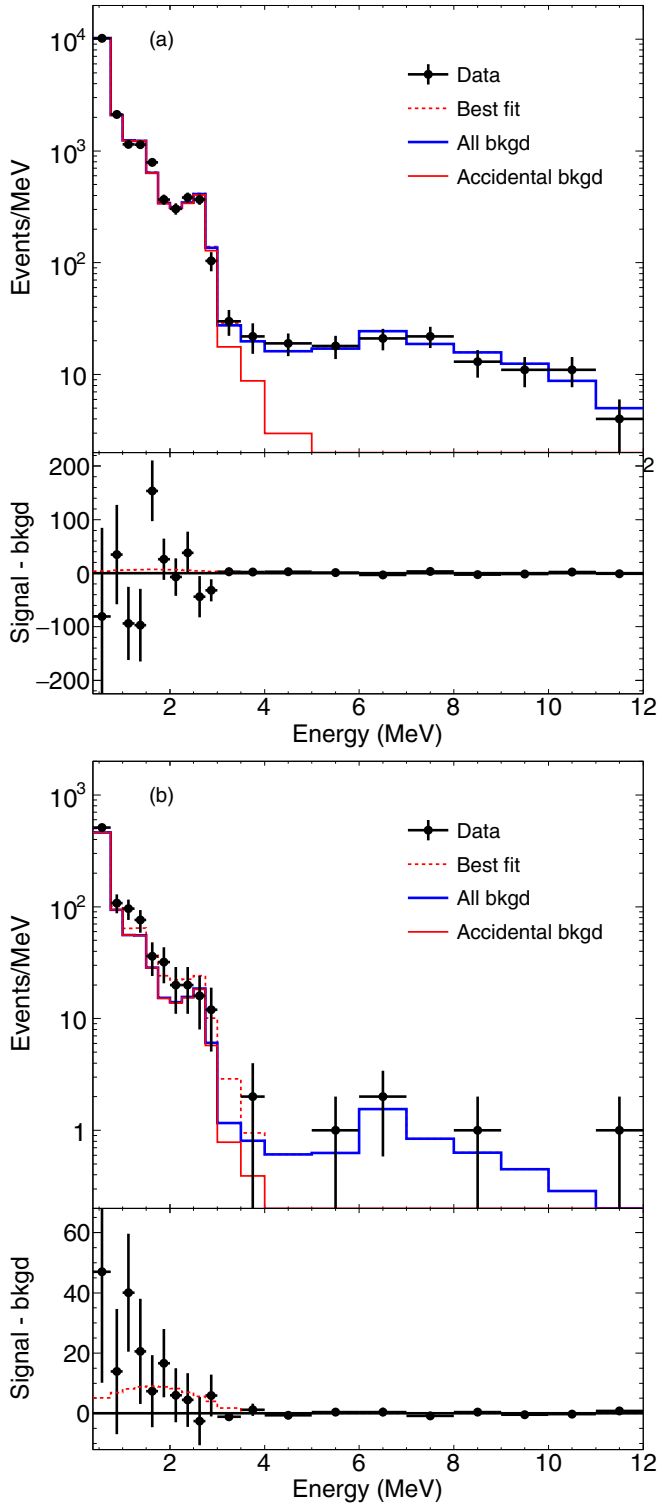

FIG. 10. (a) Fit for ^{6}He with zero neutrons. (b) Same, for one neutron. This is a display binning that combines the four neutrino target regions. The accidental background is shown in solid red. Stacked on this is the correlated background (^{8}Li and ^{16}N) in solid blue. The best fit including ^{6}He is shown in dotted red.

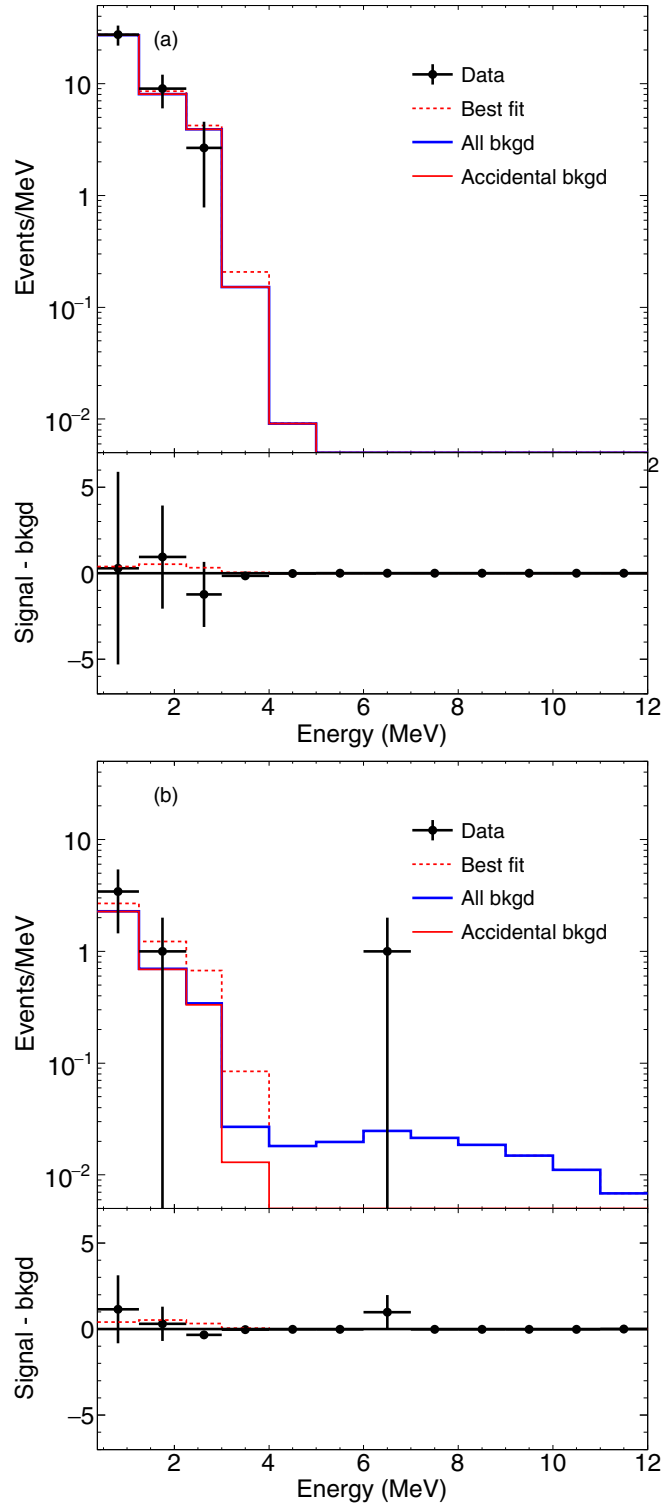

FIG. 11. (a) Fit for ^{6}He with two neutrons. (b) Same, for three neutrons. The conventions are the same as in Fig. 10.

The results are shown in Figs. 10 and 11 and Table IV. There are no clear signals, but the one-neutron case does have an excess. Without claiming to have discovered this process, we note that $^{12}\mathrm{C}(\mu^-, \nu p\alpha)^{7}$He would give this signal since ^{7}He immediately decays via neutron emission to ^{6}He. In contrast, the zero-, two-, and three-neutron final states would require less favorable combinations of charged particle emission.

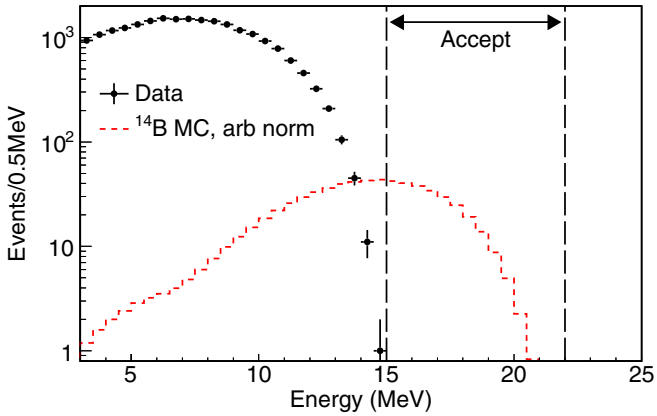

FIG. 12. Energy cut for ^{14}B search, showing no events in the signal region. The data below the cut are primarily ^{12}B.

E. ^{14}B

With its 12.5-ms half-life and extremely high Q value of 20.6 MeV, ^{14}B can be identified with very little background by looking for early events above the ^{12}B β endpoint. Events are therefore selected if the candidate decay has 15–22 MeV, occurs between 1 and 62.5 ms after the stopping muon, and within 400 mm of the stopping point. The energy cut efficiency is evaluated using β branch probabilities found at TUNL [33] and is found to be 39%. The overall efficiency is 31%. No events are observed with no background (see Fig. 12), giving a limit of $< 0.16\%$ at 90% CL for ^{16}O$(\mu^-,\nu 2p)^{14}$B, including a systematic error on the number of oxygen captures.

See Table V for a summary of isotope production results.

IX. EXCLUSIVE STATES OF ^{12}B

When ^{12}B is formed in an excited state, it is possible to observe γs from its de-excitation. This allows measurements both of the rate of transition to excited states and, by subtraction, of the ground state. Because Double Chooz has 4π coverage and good γ containment, each state can be identified unambiguously, despite the "unbelievably capricious" [1] arrangement of bound levels, giving nearly degenerate individual γ energies, that has plagued earlier measurements.

The states of ^{12}B are well known, with three relevant bound levels at 951, 1674, and 2621 keV, each of which has previously been shown to be populated by muon capture on ^{12}C. As will be shown, our data suggest that some unbound levels are also populated at a measurable rate, including 3759 keV.

A. Selection

In order to only use events for which the trigger has been shown to be fully efficient and the event energy reliable, only stopping muons depositing less than 215 MeV in the inner detector are used, this being $(38.6 \pm 0.4)\%$ of stopping muons. Also due to the behavior of the trigger, the times of the events are limited as follows:

(1) When studying 953- and 1674-keV levels, the capture must be $4\ \mu s \leqslant t < 5\ \mu s$ after the muon.

(2) For 2621 and 3759 keV, $3\ \mu s \leqslant t < 5\ \mu s$.

(3) To search for higher levels: $2\ \mu s \leqslant t < 5\ \mu s$.

TABLE V. All measurements of isotope production probabilities per nuclear muon capture in this work. All limits are set at 90% CL and include systematic errors. Protons and αs are shown as products for illustration; they are not observed. The reaction product "X" indicates several possible unobserved additional products. The ^{9}Li results assume no ^{8}He, and the ^{13}C$(\mu^-,\nu\alpha)^9$Li result assumes no contribution from ^{12}C.

Reaction	Probability/capture
^{12}C$(\mu^-,\nu 0nX)^6$He	$<0.43\%$
^{12}C$(\mu^-,\nu 1nX)^6$He	$<0.47\%$
^{12}C$(\mu^-,\nu 2nX)^6$He	$<7\times10^{-4}$
^{12}C$(\mu^-,\nu 3nX)^6$He	$<8\times10^{-4}$
^{12}C$(\mu^-,\nu 4n)^8$B	$<3.2\times10^{-5}$
^{12}C$(\mu^-,\nu\alpha)^8$Li	$[0.64 \pm 0.04(\text{stat}) \pm 0.02(\text{syst})]\%$
^{12}C$(\mu^-,\nu p)^{11}$Be	$<0.20\%$
^{12}C$(\mu^-,\nu)^{12}$B	$[17.35^{+0.21}_{-0.52}(\text{stat}) \pm 0.27(\text{syst})]\%$
$^{\text{nat}}$C$(\mu^-,\nu X)^8$He	$<7\times10^{-4}$
$^{\text{nat}}$C$(\mu^-,\nu X)^9$Li	$[2.4 \pm 0.9(\text{stat}) \pm 0.04(\text{syst})]\times10^{-4}$
^{13}C$(\mu^-,\nu n\alpha)^8$Li	$[5.1^{+1.1}_{-1.0}(\text{stat}) \pm 0.3(\text{syst})]\%$
^{13}C$(\mu^-,\nu\alpha)^9$Li	$[2.4 \pm 0.9(\text{stat}) \pm 0.05(\text{syst})]\%$
^{13}C$(\mu^-,\nu 2p)^{11}$Li	$<0.7\%$
^{13}C$(\mu^-,\nu p)^{12}$Be	$<0.20\%$
^{13}C$(\mu^-,\nu n)^{12}$B	$[51.6 \pm 5.0(\text{stat}) \pm 2.6(\text{syst})]\%$
^{13}C$(\mu^-,\nu)^{13}$B	$<40\%$
^{14}N$(\mu^-,\nu 5n)^9$C	$<3.6\%$
^{16}O$(\mu^-,\nu 2p)^{14}$B	$<0.16\%$
^{16}O$(\mu^-,\nu p6n)^9$C	$<9\times10^{-4}$
^{16}O$(\mu^-,\nu p)^{15}$C	$<9\%$
^{16}O$(\mu^-,\nu 4n)^{12}$N	$<8\times10^{-4}$

Using the bound muon lifetime, these timing requirements have efficiencies of 5.5%, 14.3%, and 28.6%, respectively.

To reduce background from other processes, notably ^{12}C$(\mu^-,\nu n)^{11}$B*, it is necessary to require observation of the ^{12}B β decay as well as the γs. These events are selected in a similar way as in Sec. IV, with the additional requirements that the decay be between 2 and 60 ms after the stopping muon and reconstruct within 400 mm of the muon endpoint. By requiring the β decay to occur 2 ms after the muon stop, we avoid selecting neutron captures as ^{12}B.

Given these requirements, the overall efficiency is 1.09% for selection 1, 4.14% for selection 2, and 6.8% for selection 3, with 1.5% relative error on each, with the requirements on muon energy and γ timing being the main drivers.

Selected events are shown in Fig. 13. The 2621- and 952-keV levels are clearly visible. The 1674-keV level is not so clear, but fortunately is already known to be present.

There are also four events in selection 2 between 3500 and 4000 keV, which may be due to the 3759-keV level. This level is known to de-excite via γ emission some fraction of the time [34]. It is therefore included in the fits below. Further, in selection 3 there are six events between 5800 and 7400 keV, which also rises well above background. One possibility is that these originate from the 6600-keV level of ^{12}B, but as this assignment seems less clear, we simply note that it appears that other states are populated to some extent. Similarly, the

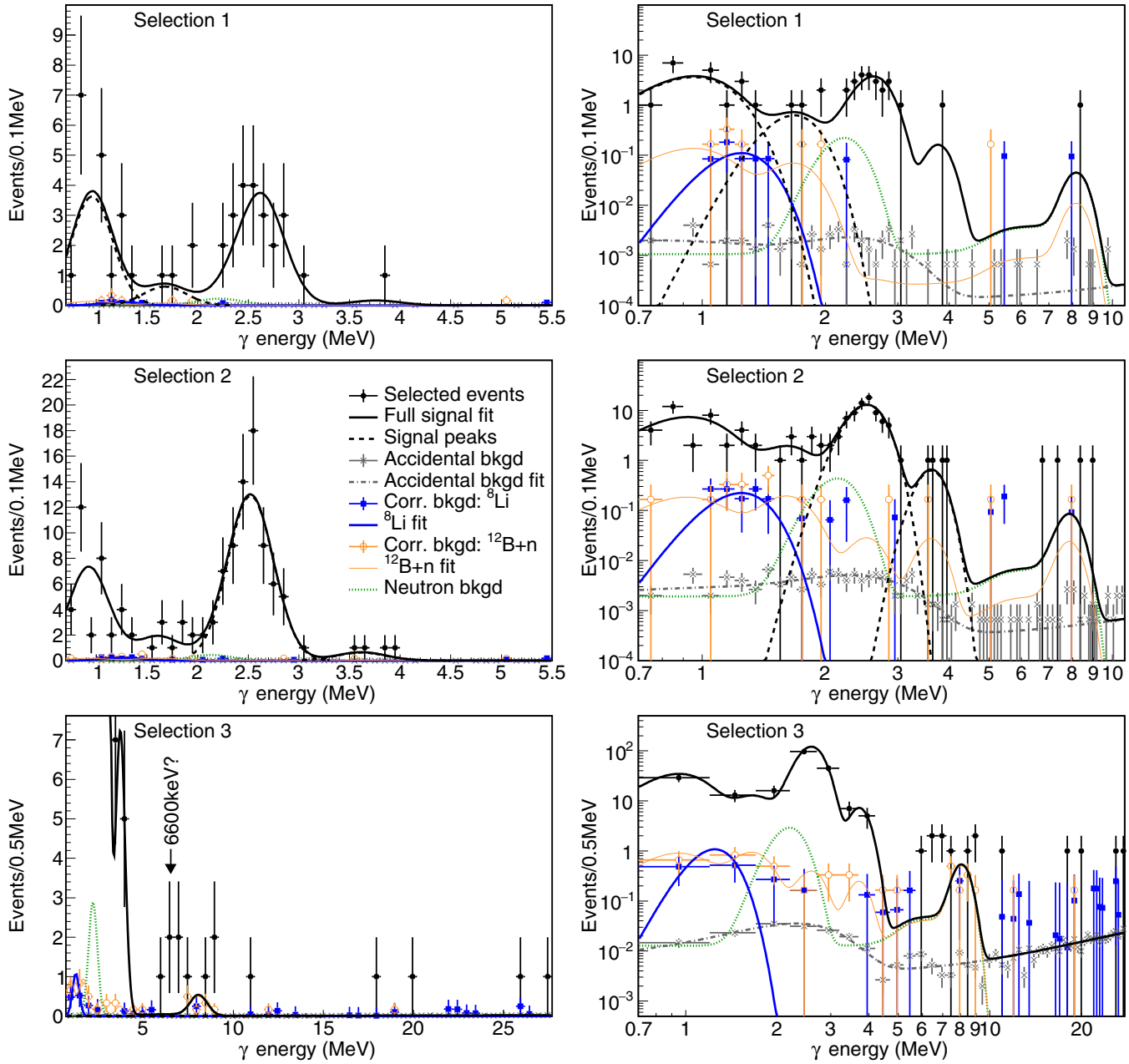

FIG. 13. ^{12}Bγ spectra for each selection, shown on a linear scale on the left and a log scale on the right. Selected events and the overall fit are shown in black with filled circles and a thick solid line, the signal components of the fit with a dashed black line, accidental background (Sec. IX B 1) in gray with crosses and a dot-dashed line, correlated background from non-^{12}B isotopes assumed to be all ^{8}Li (Sec. IX B 2) in blue with squares and a triple-dot-dashed line, and from early neutron captures following ^{13}C$(\mu^-,\nu n)^{12}$B selected as γs (Sec. IX B 5) with a green dashed line. The data and fit for ^{13}C$(\mu^-,\nu n)^{12}$B* (Sec. IX B 3) is shown in orange with open circles and a thin solid line and is scaled to the level at which it acts as a background to ^{12}C$(\mu^-,\nu)^{12}$B*. The fit line includes the spallation background to ^{13}C$(\mu^-,\nu n)^{12}$B itself (Sec. IX B 4), visible at the Gd-n energy, which does not affect ^{12}C$(\mu^-,\nu)^{12}$B.

five events between 10 and 25 MeV are significantly over the background of 0.15 events.

B. Fit

Figure 13 shows the fits used to extract the number of events at each level. The fit for selection 1 is used to find the number of 953- and 1674-keV events, while that for selection 2 is used to find the number of 2621- and 3759-keV events. The fit for selection 3 is used only to demonstrate the level of consistency of the higher energy data with expectations. The fit includes terms for each of the following, which will be explained in detail in the following sections:

(i) The signal: γs from $^{12}\mathrm{C} \rightarrow {}^{12}\mathrm{B}^{*} \rightarrow {}^{12}\mathrm{B}_{\mathrm{g.s.}}\,\gamma$.

(ii) Accidental background from the sequence (1) stopping muon track, (2) muon decay, (3) accidental ^{12}B-like event. Event (2) is selected as the γ, giving a Michel spectrum.

(iii) Accidental background from the sequence (1) stopping muon track—the muon creates ^{12}B in the ground state (2) accidental γ-like event (3) ^{12}B decay. This gives an accidental spectrum mostly at low energy from detector radioactivity.

(iv) Correlated background from $^{13}\mathrm{C} \rightarrow {}^{8}\mathrm{Li}^{*}$.

(v) Correlated background from $^{13}\mathrm{C} \rightarrow {}^{12}\mathrm{B}^{*} + n$, where the neutron is lost.

(vi) Correlated background from $^{13}\mathrm{C} \rightarrow {}^{12}\mathrm{B}_{\mathrm{g.s.}} + n$, in which the neutron captures early and is selected as the γ.

(vii) Background from through-going muons producing ^{12}B and several neutrons via spallation.

Following the sections on each background, additional systematics are discussed.

1. Accidentals

The accidental spectrum was derived by repeating the selection with the timing window for ^{12}B β decays shifted to be a long time after the muon. Many windows were used to give a high-statistics determination of the spectrum. The accidentals characterized in this way include both the case of an uncorrelated γ (up to ~3 MeV) with a real ^{12}B decay, and the case of a Michel electron with an uncorrelated ^{12}B candidate.

2. Correlated background: ^{8}Li

From Sec. VIII A, it is known that ^{8}Li is produced in significant quantities. It has one bound level at 981 keV. No previous results are available on the rate of transition to particular states. β decays of ^{8}Li will be selected with about the same efficiency as ^{12}B if they fall into the 2–60-ms selection window. However, the much longer half-life of ^{8}Li puts only a small fraction in this window. Because ^{8}Li is produced with an α, the visible energy is the sum of that from the α and γ. Given our measurements of scintillator quenching, and assuming a mean α energy of 4.5 MeV [30, Fig. 5(b)], the total visible energy expected is 1.23 MeV.

The contribution from ^{8}Li(981) is determined by selecting events as in Sec. IX A, but with a β decay window of 0.3–4.2 s after the muon. The significance of the presence of these γs is 2σ. Limits are obtained, and are shown in Table VIII. The central value, scaled to the number expected in the ^{12}B time window, is input into the ^{12}B fit and the errors used as a pull term.

Other isotopes were considered for this treatment. No significant background to the three bound ^{12}B levels from ^{13}B is expected, since ^{13}B's first excited state is at 3483 keV. It is possible that the four events tentatively attributed to ^{12}B(3759) are instead ^{13}B(3483); the energies are more compatible with the former, but not enough information is available to confidently distinguish the possibilities.

Other known products of muon capture are disfavored because their long lifetimes and/or low production rates will reduce their contribution to negligible levels. For instance, only 0.6% of ^{16}N β decays will be within the selected time window. The bound levels of ^{16}N's are all below 400 keV. It has unbound levels at 3353, 3523, and 3963 keV, but even if these accounted for 100% of ^{16}N production, the background contribution would be well under one event, particularly since they are known to de-excite primary by neutron emission.

There is one bound level in ^{9}Li, at 2691 keV, but because the production rate is so low, even if it was produced in this state 100% of the time, we would only expect to select about 0.3 events. Other isotopes yield even lower background rates regardless of what assumptions are made.

3. Correlated background: $^{13}\mathrm{C} \rightarrow {}^{12}\mathrm{B}{+}n$

No previous results are available for the reaction $^{13}\mathrm{C}(\mu^{-},\nu n)^{12}\mathrm{B}$, so there is no constraint on the exclusive rates to each ^{12}B state in this process. In the case of this analysis, the neutron efficiency is high, $(85.8 \pm 1.0)\%$, and the probability of selecting an event as a neutron when no true neutron is present is low, 1.1×10^{-4}, which means the ^{12}C and ^{13}C variants can be largely separated.

Events with and without neutrons are therefore both selected and a simultaneous fit is performed with both samples, with ^{13}C and ^{12}C processes on equal footing. The fit includes the neutron efficiency as a parameter, which is constrained by a 1% pull term. The fit results for $^{13}\mathrm{C}(\mu^{-},\nu n)^{12}\mathrm{B}$ are shown in Table VII. Because there are so few events, none of the lines is confidently observed. However, upper limits can be set. No unitarity condition is applied (i.e. the fit allows the levels to

TABLE VI. Transition rates to each ^{12}B level measured in the reactions $^{12}\mathrm{C}(\mu^{-},\nu)^{12}\mathrm{B}^{(*)}$. For 3759 keV, this is the probability of reaching the level *and* de-exciting via γ emission; it is assumed that no other γ lines contribute.

Daughter	Rate (10^{3} s^{-1})	Per ^{12}B β decay (%)	Significance
^{12}B(g.s.)	$5.68^{+0.13}_{-0.22}(\mathrm{stat}) \pm 0.06(\mathrm{syst})$ $^{+0.14}_{-0.23}(\mathrm{total})$		
^{12}B*(953)	$0.31^{+0.09}_{-0.07}(\mathrm{stat}) \pm 0.01(\mathrm{syst})$ $^{+0.09}_{-0.07}(\mathrm{total})$	$4.8^{+1.3}_{-1.1}(\mathrm{stat})^{+0.2}_{-0.1}(\mathrm{syst})$ $^{+1.3}_{-1.1}(\mathrm{total})$	6.2σ
^{12}B*(1674)	$0.06^{+0.04}_{-0.03}(\mathrm{stat}) \pm 0.003(\mathrm{syst})$ $^{+0.04}_{-0.03}(\mathrm{total})$	$0.9^{+0.7}_{-0.5}(\mathrm{stat})^{+0.05}_{-0.04}(\mathrm{syst})$ $^{+0.7}_{-0.5}(\mathrm{total})$	1.6σ
^{12}B*(2621)	$0.47^{+0.06}_{-0.05}(\mathrm{stat}) \pm 0.01(\mathrm{syst})$ $^{+0.06}_{-0.05}(\mathrm{total})$	$7.1^{+0.9}_{-0.8}(\mathrm{stat})^{+0.2}_{-0.1}(\mathrm{syst})$ $^{+0.9}_{-0.8}(\mathrm{total})$	15.3σ
^{12}B*(3759)	$0.026^{+0.015}_{-0.011}(\mathrm{stat}) \pm 0.001(\mathrm{syst})$ $^{+0.015}_{-0.011}(\mathrm{total})$	$0.39^{+0.23}_{-0.17}(\mathrm{stat}) \pm 0.01(\mathrm{syst})$ $^{+0.23}_{-0.17}(\mathrm{total})$	2.8σ

TABLE VII. Transition rates for each ^{12}B level measured in the reactions $^{13}C(\mu^-,\nu n)^{12}B^*$. The limits are taken as the primary results. They result from a Bayesian analysis that takes a flat prior from 0 to 100%. Because it is assumed that any or all of the events are background, none of the levels are imposed as constraints on the probabilities of other levels.

Daughter	Rate (10^3 s^{-1})	Per ^{12}B β decay (%)	Significance
$^{12}B^*(953)+n$	8^{+5}_{-4}(stat) $\pm$ 0.2(syst)	46^{+29}_{-21}(stat) $\pm$ 4(syst)	3.0σ
	<15 at 90% CL	**<80. at 90% CL**	
$^{12}B^*(1674)+n$	5^{+4}_{-3}(stat) $\pm$ 0.1(syst)	25^{+22}_{-14}(stat) $\pm$ 2(syst)	1.6σ
	<9.9 at 90% CL	**<54 at 90% CL**	
$^{12}B^*(2621)+n$	$0.7^{+1.1}_{-0.6}$(stat) $\pm$ 0.02(syst)	4^{+6}_{-3}(stat) $\pm$ 0.3(syst)	1.2σ
	<2.2 at 90% CL	**<12 at 90% CL**	
$^{12}B^*(3759)+n$	$0.8^{+1.1}_{-0.6}$(stat) $\pm$ 0.02(syst)	4^{+6}_{-3}(stat) $\pm$ 0.4(syst)	1.8σ
	<2.2 at 90% CL	**<12 at 90% CL**	

add up to more than 100% of the ^{12}B $+n$ production), making the limits conservative.

Assuming no unaccounted-for background, the total fraction of ^{12}B produced from ^{13}C in an excited state is $[78^{+34}_{-21}(\text{stat}) \pm 8(\text{syst})]\%$. This is much higher than the probability for ^{12}B produced from ^{12}C to be in an excited state, but the production mechanism is different so they cannot be compared directly. In a naive shell model, $^{13}C(\mu^-,\nu n)^{12}B$ involves removing a proton from an inner shell 2/3 of the time, whereas in $^{12}C(\mu^-,\nu)^{12}B$, no nucleons are removed.

4. Background: Spallation

The following sequence of events can also contribute a background at the H-n and Gd-n energies and would appear in the $^{13}C(\mu^-,\nu n)^{12}B$ sample: (1) through-going muon, selected as a stopping muon, that produces three or more neutrons through spallation; one makes ^{12}B through the (n,p) reaction, (2) another neutron captures on hydrogen or gadolinium and is selected as a γ, (3) a third neutron capture is correctly selected as such, (4) the ^{12}B β decays.

Lacking an estimate for the rate of this sequence, it is taken into account by including free parameters in the fit that controls the contribution at the H-n and Gd-n energies in the ^{12}B $+n$ sample. There does seem to be Gd-n present, primarily visible in selection 3 (with one event in selection 2), but the fit finds no H-n component in any selection. The uncertainty on this is propagated through the fit.

Since this sequence is therefore observed to be rare, and spallation typically produces many neutrons, the corresponding sequence without event (3), the third neutron capture, which would instead contaminate the $^{12}C(\mu^-,\nu)^{12}B$ sample, is assumed to be negligible, particularly because it is much more likely for a single neutron to be captured during the longer neutron selection time window than the γ time window.

5. Correlated background: $^{13}C(\mu^-,\nu n)^{12}B$ neutrons selected as γs

If the neutron from $^{13}C(\mu^-,\nu n)^{12}B$ captures within the γ time window, the event will be selected as $^{12}C(\mu^-,\nu)^{12}B$ with a γ energy of 2225 keV. Using the measured rate of this reaction from Sec. IV and the probabilities of capture within the γ timing window, about 1.2 H-n events and 0.7 GD-n events are expected for selection 1, $2.4+1.3$ for selection 2, and $3.5+1.7$ for selection 3. These rates are included in the fit as fixed amounts. They are not allowed to vary in the fit because any ^{12}B levels below 10 MeV that are not included in the fit will spuriously pull the neutron rate up. Instead, a systematic error is assigned after the fact, as shown below.

As a cross-check on the rate of H-n events contaminating the 2621-keV line, the timing distribution of these γ candidates was fit for a combination of the bound μ^- lifetime and the neutron capture lifetime. No evidence of a neutron timing component was found, with a limit from timing alone of less than 25% neutron contamination at 90% CL.

C. Results and systematics

Numerical results are shown in Tables VI–VIII. These include the rate for ground state $^{12}C(\mu^-,\nu)^{12}B$, which is found by subtracting the excited state rates from the total rate. To cover the possibility that the 3759-keV measurement is spurious, its contribution is allowed to vary from zero to the stated value in this calculation. Likewise, to cover the possibility that higher energy states also cascade down to the ground state, an error is added that covers the possibility that all the events from 5 to 30 MeV in Fig. 13 are such events. Both of these effects are small compared to the statistical error.

In the tables, all sources of error handled directly in the fit are considered to be statistical. The additional systematic errors are as follows:

(i) For results stated as a fraction of ^{12}B production, many systematic errors cancel, leaving an efficiency error of 1.1%, primarily due to the muon energy cut. The statistical error on the total rate of $^{12}C(\mu^-,\nu)^{12}B$ found in Sec. IV applies, giving an additional systematic of $^{+3.0}_{-1.2}$% relative.

(ii) For results stated as a transition rate, the entire 1.5% efficiency error from Sec. IX A applies, as does the error on the number of atomic captures on ^{12}C, 1.4% (see Sec. V), plus a very small 0.1% error from the μ^- lifetime in ^{12}C.

TABLE VIII. Rate for the exclusive reaction $^{12}C(\mu^-,\nu\alpha)$ ^{8}Li*(981). The methodology is the same as in Table VII.

Daughter	Rate (10^3 s^{-1})	Per ^{8}Li β decay (%)
^{8}Li*(981)	$0.10 \pm 0.05(\text{stat}) \pm 0.002(\text{syst})$	$40 \pm 20(\text{stat}) \pm 3(\text{syst})$
	<0.16 at 90% CL	**<67% at 90% CL**

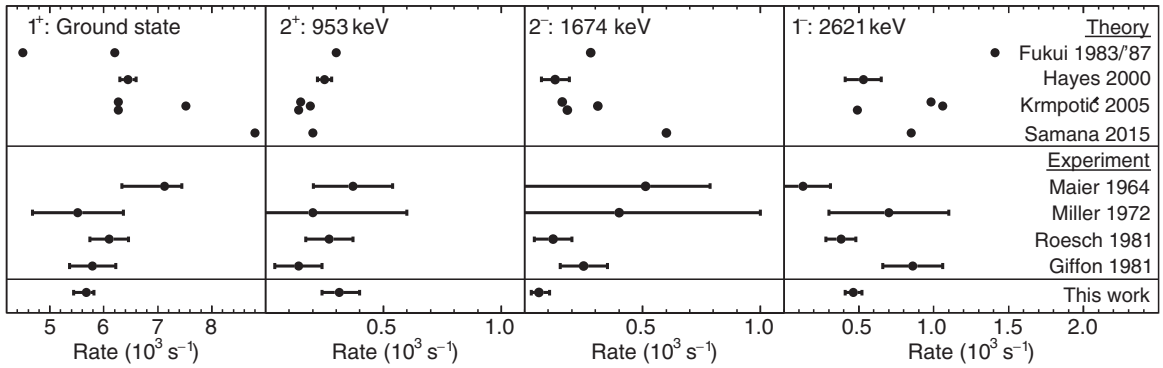

FIG. 14. Comparison of results for each bound state of ^{12}B to theory (from top to bottom: [1,2,35–38]) and previous measurements ([20,29,39,40]). Krmpotić [2] presents three parametrizations of PQRPA; all are displayed here. Each of the more recent experiments depends on Maier [20] for the total rate, but here is shown updated using the Double Chooz total rate. Maier's result has itself been corrected here to account for their ^{13}C fraction and to correct an error in their calculations. Giffon [40] is reanalyzed to remove the erroneous assumption that the 953-keV level is negligible. One experiment [41] has been excluded due to having made the same assumption and there being insufficient information to reanalyze.

(iii) An additional overall systematic on each level is assigned for uncertainty in the energy reconstruction following a muon. The relative uncertainties in the event counts from this effect are 0.5% for 953 keV, 2.8% for 1674 keV, 0.2% for 2621 keV, and 1.7% for 3597 keV.

(iv) To account for uncertainties in the number of H-n captures assumed in Sec. IX B 5, a further systematic error is assigned to the two adjacent levels. This is evaluated to be 1% relative for 2621 keV and 3% relative for 1674 keV.

All systematics combined are much smaller than the statistical error, which for the most precise level is 12% relative.

These results are compared to previous experimental and theoretical work in Fig. 14. Note particularly the comparison of these results to the PQRPA model, which is also used to generate neutrino cross sections. For instance, for their *parametrization III* (the bottom points shown for Krmpotić 2005) the ground state prediction is 4σ high of our measurement (experimental errors only), the 953-keV level is 2σ low, the 1674-keV level is 2σ high, and the 2621-keV level is in good agreement.

X. SUMMARY

Using the Double Chooz neutrino detector, the probabilities of final states of muon capture on carbon, nitrogen, and oxygen have been measured. One set of reactions, $^{12}\mathrm{C}(\mu^-,\nu)^{12}\mathrm{B}^{(*)}$, has been observed before; more precise results are reported here. Other reactions have been observed for the first time, and limits on several more have been set.

The near detector is now also taking data. Because it has an overburden of 120-m water equivalent, it receives several times the flux of muons as compared to the far detector. This flux is also softer, giving a higher fraction of stopping muons. This provides an excellent data set for future analysis of relatively short-lived isotopes.

The RENO [42] and Daya Bay [43] detectors have similar capabilities as Double Chooz and could also perform these measurements. Similarly, a possibility to increase world data on muon capture in oxygen comes from Super-Kamiokande, which has collected a large sample of stopping muons in water [44], but has thus far treated them only as a background to spallation studies.

The observed rate of βn decays shows that stopping muons do not form a significant background to θ_{13} measurements at any of the current facilities. Since the ratio of stopping to through-going muons rises as the amount of overburden decreases, it is possibly a relevant background for inverse β decay detectors with very small overburdens, such as those investigating the reactor neutrino anomaly [45].

ACKNOWLEDGMENTS

We thank the French electricity company EDF; the European fund FEDER; the Région de Champagne Ardenne; the Département des Ardennes; and the Communauté de Communes Ardenne Rives de Meuse. We acknowledge the support of the CEA, CNRS/IN2P3, the computer center CCIN2P3, and LabEx UnivEarthS in France (ANR-11-IDEX-0005-02); the Ministry of Education, Culture, Sports, Science and Technology of Japan (MEXT) and the Japan Society for the Promotion of Science (JSPS); the Department of Energy and the National Science Foundation of the United States; U.S. Department of Energy Award No. DE-NA0000979 through the Nuclear Science and Security Consortium; the Ministerio de Economía y Competitividad (MINECO) of Spain; the Max Planck Gesellschaft, and the Deutsche Forschungsgemeinschaft DFG, the Transregional Collaborative Research Center TR27, the excellence cluster "Origin and Structure of the Universe", and the Maier-Leibnitz-Laboratorium Garching in Germany; the Russian Academy of Science, the Kurchatov Institute and RFBR (the Russian Foundation for Basic Research); the Brazilian Ministry of Science, Technology and Innovation (MCTI), the Financiadora de Estudos e Projetos (FINEP), the Conselho Nacional de Desenvolvimento Científico e Tecnológico (CNPq), the São Paulo Research Foundation (FAPESP), and the Brazilian Network for High Energy Physics (RENAFAE) in Brazil.

[1] D. F. Measday, Phys. Rep. **354**, 243 (2001).
[2] F. Krmpotić, A. Samana, and A. Mariano, Phys. Rev. C **71**, 044319 (2005).
[3] T. Gorringe and H. W. Fearing, Rev. Mod. Phys. **76**, 31 (2004).
[4] Y. Abe *et al.* (Double Chooz), J. High Energy Phys. 10 (2014) 086.
[5] T. J. Stocki, D. Measday, E. Gete, M. Saliba, B. Moftah, and T. Gorringe, Nucl. Phys. A **697**, 55 (2002).
[6] D. F. Measday and T. J. Stocki, in *VII Latin American Symposium on Nuclear Physics and Applications*, AIP Conf. Proc. No. 947, edited by R. Alarcon, P. L. Cole, C. Djalali, and F. Umeres (AIP, Melville, NY, 2007), p. 253.
[7] National Nuclear Data Center, "Chart of Nuclides database", www.nndc.bnl.gov/chart (2015), accessed: 2015-10-21.
[8] C. Aberle, C. Buck, F. X. Hartmann, S. Schonert, and S. Wagner, JINST **6**, P11006 (2011).
[9] C. Aberle, C. Buck, B. Gramlich, F. X. Hartmann, M. Lindner, S. Schönert, U. Schwan, S. Wagner, and H. Watanabe, J. Instrum. **7**, P06008 (2012).
[10] T. Suzuki, D. F. Measday, and J. P. Roalsvig, Phys. Rev. C **35**, 2212 (1987).
[11] P. Antonioli, C. Ghetti, E. V. Korolkova, V. A. Kudryavtsev, and G. Sartorelli, Astropart. Phys. **7**, 357 (1997).
[12] P. Adamson *et al.* (MINOS), Phys. Rev. D **76**, 052003 (2007).
[13] P. Adamson *et al.* (MINOS), Phys. Rev. D **83**, 032011 (2011).
[14] P. Achard *et al.*, Phys. Lett. B **598**, 15 (2004).
[15] T. K. Gaisser, Astropart. Phys. **35**, 801 (2012).
[16] M. Guan, M. Chu, J. Cao, K. Luk, and C. Yang, arXiv:1509.06176.
[17] Y. Abe *et al.* (Double Chooz), Nucl. Instrum. Methods Phys. Res. A **764**, 330 (2014).
[18] A. Czarnecki, M. Dowling, X. Garcia i Tormo, W. J. Marciano, and R. Szafron, Phys. Rev. D **90**, 093002 (2014).
[19] D. Atwood and W. J. Marciano, Phys. Rev. D **41**, 1736 (1990).
[20] E. J. Maier, R. M. Edelstein, and R. T. Siegel, Phys. Rev. **133**, B663 (1964).
[21] F. Ajzenberg-Selove, Nucl. Phys. A **506**, 1 (1990).
[22] F. Ajzenberg-Selove and C. L. Busch, Nucl. Phys. A **336**, 1 (1980).
[23] C. W. Cook, W. A. Fowler, C. C. Lauritsen, and T. Lauritsen, Phys. Rev. **107**, 508 (1957).
[24] D. E. Alburger and A. M. Nathan, Phys. Rev. C **17**, 280 (1978).
[25] G. K. Schenter and P. Vogel, Nucl. Sci. Eng. (United States) **83**, 393 (1983).
[26] H. A. Weidenmüller, Rev. Mod. Phys. **33**, 574 (1961).
[27] H. Daniel, Rev. Mod. Phys. **40**, 659 (1968).
[28] R. Barlow, Nucl. Instrum. Methods Phys. Res. A **297**, 496 (1990).
[29] L. Ph. Roesch, N. Schlumpf, D. Taqqu, V. L. Telegdi, P. Truttmann, and A. Zehnder, Phys. Lett. B **107**, 31 (1981).
[30] H. Morinaga and W. F. Fry, Il Nuovo Cimento **10**, 308 (1953).
[31] Y. Abe *et al.* (Double Chooz), J. High Energy Phys. 01 (2016) 163.
[32] L. Demortier, Objective Bayesian upper limits for poisson processes, CDF/MEMO/STATISTICS/PUBLIC/5928 (2005).
[33] TUNL, Nuclear data evaluation project, www.tunl.duke.edu/nucldata/ (2015), accessed: 2015-07-08.
[34] TUNL, ^{12}B table of adopted levels, www.tunl.duke.edu/nucldata/HTML/A=12/12_02_1990.pdf, accessed: 2015-07-08.
[35] M. Fukui, T. Sato, H. Ohtsubo, M. Morita, and K. Koshigiri, Prog. Theor. Phys. **70**, 827 (1983).
[36] M. Fukui, T. Sato, H. Ohtsubo, M. Morita, and K. Koshigiri, Prog. Theor. Phys. **78**, 343 (1987).
[37] A. C. Hayes and I. S. Towner, Phys. Rev. C **61**, 044603 (2000).
[38] A. R. Samana, D. Sande, and F. Krmpotić, in *NuINT12: The 8th International Workshop on Neutrino-nucleus Interactions in the Few-GeV Region*, AIP Conf. Proc. No. 1663, edited by H. da Motta, J. G. Morfin, and M. Sakuda (AIP, New York, 2015), p. 120003.
[39] G. H. Miller, M. Eckhause, F. R. Kane, P. Martin, and R. E. Welsh, Phys. Lett. B **41**, 50 (1972).
[40] M. Giffon, A. Goncalves, P. A. M. Guichon, J. Julien, L. Roussel, and C. Samour, Phys. Rev. C **24**, 241 (1981).
[41] Yu. G. Budyashov, V. G. Zinov, A. D. Konin, S. V. Medved, A. I. Mukhin, E. B. Ozerov, A. M. Chatrchyan, and R. Z. Eramzhyan, J. Exp. Theor. Phys. **31**, 651 (1970).
[42] J. K. Ahn, S. Chebotaryov, J. H. Choi, S. Choi, W. Choi, Y. Choi, H. I. Jang, J. S. Jang, E. J. Jeon, I. S. Jeong, K. K. Joo, B. R. Kim, B. C. Kim, H. S. Kim, J. Y. Kim, S. B. Kim, S. H. Kim, S. Y. Kim, W. Kim, Y. D. Kim, J. Lee, J. K. Lee, I. T. Lim, K. J. Ma, M. Y. Pac, I. G. Park, J. S. Park, K. S. Park, J. W. Shin, K. Siyeon, B. S. Yang, I. S. Yeo, S. H. Yi, and I. Yu (RENO), Phys. Rev. Lett. **108**, 191802 (2012).
[43] F. P. An *et al.* (Daya Bay), Chin. Phys. C **37**, 011001 (2013).
[44] Y. Zhang *et al.* (Super-Kamiokande), Phys. Rev. D **93**, 012004 (2016).
[45] G. Mention, M. Fechner, T. Lasserre, T. A. Mueller, D. Lhuillier, M. Cribier, and A. Letourneau, Phys. Rev. D **83**, 073006 (2011).